Bulseco Ashley (Orcid ID: 0000-0001-5322-3070)
Spivak Amanda (Orcid ID: 0000-0001-6743-0783)

Metagenomics coupled with biogeochemical rates measurements provide evidence that nitrate addition stimulates respiration in salt marsh sediments

Ashley N. Bulseco[1], Joseph H. Vineis[2], Anna E. Murphy[2], Amanda C. Spivak[3], Anne E. Giblin[1], Jane Tucker[1], and Jennifer L. Bowen[2]*

[1]The Ecosystems Center, Marine Biological Laboratory, Woods Hole, MA 02543

[2]Department of Marine and Environmental Sciences Marine Science Center, Northeastern University, Nahant, MA 01908

[3]Department of Marine Sciences, Franklin College of Arts and Sciences, University of Georgia, Athens, GA 30602

Corresponding author:

Jennifer Bowen, Department of Marine and Environmental Sciences, Marine Science Center, Northeastern University, MA 01908, Phone: 617-373-2059, Email: je.bowen@northeastern.edu

This is the author manuscript accepted for publication and has undergone full peer review but has not been through the copyediting, typesetting, pagination and proofreading process, which may lead to differences between this version and the Version of Record. Please cite this article as doi: 10.1002/lno.11326

Abstract:

High throughput sequencing has enabled robust shotgun metagenomic sequencing that informs our understanding of the genetic basis of important biogeochemical processes. Slower to develop, however, are the application of these tools in a controlled experimental framework that pushes the field beyond exploratory analysis towards hypothesis-driven research. We performed flow-through reactor experiments to examine how salt marsh sediments from varying depths respond to nitrate addition and linked biogeochemical processes to this underlying genetic foundation. Understanding the mechanistic basis of carbon and nitrogen cycling in salt marsh sediments is critical for predicting how important ecosystem services provided by marshes, including carbon storage and nutrient removal, will respond to global change. Prior to the addition of nitrate, we used metagenomics to examine the functional potential of the sediment microbial community that occurred along a depth gradient, where organic matter reactivity changes due to decomposition. Metagenomic data indicated that genes encoding enzymes involved in respiration, including denitrification, were higher in shallow sediments, and genes indicative of resource limitation were greatest at depth. After 92 days of nitrate enrichment, we measured cumulative increases in dissolved inorganic carbon production, denitrification, and dissimilatory nitrate reduction to ammonia; these rates correlated strongly with genes that encode essential enzymes in these important pathways. Our results highlight the importance of controlled experiments in linking biogeochemical rates to underlying genetic pathways. Further,

they indicate the importance of nitrate as an electron acceptor in fueling microbial respiration, which has consequences for carbon and nitrogen cycling and fate in coastal marine systems.

Introduction:

Microorganisms are major drivers of ecosystem function, catalyzing many of Earth's biogeochemical transformations such as the carbon, nitrogen, and sulfur cycles (Falkowski 2008). Given the importance of understanding these transformations and equipped with rapid advances in sequencing technology (van Dijk et al. 2014), researchers have devoted tremendous effort towards characterizing microbial communities, from examining community structure (Graham et al. 2016) and diversity (Powell et al. 2015) using marker genes such as 16S ribosomal RNA (Woese & Fox 1977), to examining metabolic potential, function, and activity using a variety of 'omic techniques (Quince et al. 2017).

Recently, researchers have worked towards linking characteristics of the microbial community (i.e. metabolic potential, diversity, structure, etc.) to ecosystem function in order to extrapolate across spatial and temporal scales and predict ecosystem response to global environmental change (Wallenstein & Hall 2012; Reed et al. 2014). However, achieving explicit coupling between microbial communities and biogeochemical process rates remains challenging. For instance, stochastic assembly (Nemergut et al. 2013; Knelman & Nemergut 2014) and dormancy/inactivity (Jones & Lennon 2010; Lennon & Jones 2011) may hinder our ability to

predict ecosystem function by altering interactions among active portions of the microbial community. Disconnect over space and time, particularly in dynamic and spatially heterogeneous habitats, can decouple microbial community characteristics and process rates. Thus, sampling resolution and the need to aggregate and interpolate among data points may influence our ability to infer ecologically meaningful patterns (Bier et al. 2015). Further, sediment systems are incredibly diverse and complex environments that require deep sequencing to sufficiently characterize the microbial community (Lozupone & Knight 2007). We can account for some of these issues by designing enrichment experiments that aim to test explicit hypotheses under controlled environmental conditions (Prosser 2015; Hug & Co 2018), thereby avoiding strictly exploratory analyses and working towards a more targeted understanding of the microbial role in ecosystem function (Morales et al. 2011; Prosser et al. 2007).

Salt marshes and other detritus-based ecosystems are valuable platforms for testing relationships between microbial communities and ecosystem functioning related to carbon and nitrogen cycles. In addition to harboring a high diversity and abundance of microorganisms, upwards of 10^9 cells per gram of sediment, salt marshes provide several microbially-mediated ecosystem services that result in high monetary valuation, despite occupying only a small portion of coastal area (Barbier et al. 2011; Himes-Cornell et al. 2018). Carbon storage is a key ecosystem service provided by salt marshes that depends on high aboveground productivity and slow belowground decomposition due to anaerobic sediments (Mendelssohn & Morris 2000; Zedler & Kercher 2005; Mcleod et al. 2011). Organic matter (OM) accumulating at the surface

and in the rooting zone of marshes is more available to microbes than OM in deeper sediments, where OM is slow to decompose due to a combination of the chemical complexity of the OM and lower energy yield of anaerobic respiration as redox conditions change with depth (Mueller et al. 2016). Thus, as marshes accrete, the OM buried deeper belowground tends to be less reactive and is stored for long periods of time.

Salt marshes also intercept nutrient pollution from land-derived sources. Nitrogen concentrations in freshwater inputs to marshes, particularly in the form of nitrate (NO_3^-), have been increasing at an alarming rate (Galloway et al. 2017). Greater availability of NO_3^- could potentially diminish the carbon storage capacity of salt marsh sediments as NO_3^- is an energetically favorable electron acceptor compared to sulfate (SO_4^{2-}), and hence stimulates subsurface microbial respiration where OM is oxidized to fuel heterotrophic processes (Bulseco et al. 2019). A number of studies have documented how microbes respond to increased NO_3^- supply, either through shifts in the active bacterial community (Kearns et al. 2016), increased diversity and abundance of putative fungal denitrifiers (Kearns et al. 2018), or increased functional potential for denitrification (Graves et al. 2016). Several studies have also observed changes to ecosystem function in response to NO_3^-, including increased rates of denitrification and dissimilatory NO_3^- reduction to ammonium (DNRA; Koop-Jakobsen & Giblin 2010). However, to our knowledge, no study has linked these shifts in functional potential of the microbial community to changes in biogeochemical rates and distinct genetic pathways in response to NO_3^- addition.

We used a targeted, metagenomic approach to explicitly test the effect of NO_3^- enrichment on salt marsh sediment OM decomposition using controlled flow-through experiments. We first examined pre-treatment sediments and hypothesized a greater abundance of microbial functions associated with respiration in surface sediments, where OM is more reactive, and a transition to functions associated with less energetically favorable processes, such as fermentation, sulfate reduction, and methanogenesis, in deeper sediments where oxygen is not readily available. Secondly, we hypothesized that adding NO_3^- would enhance respiration by stimulating dissimilatory NO_3^- reduction processes, such as denitrification and DNRA, regardless of sediment depth. Lastly, we hypothesized that shifts in process rates, across sediment depth horizons and in response to NO_3^- additions, would coincide with changes in abundance of relevant genes involved in SO_4^{2-} reduction (i.e., *dsrB*), denitrification (i.e., nitrite (NO_2^-) and nitrous-oxide reductase), and DNRA (i.e., NO_3^- reductase) due to a shift in the metabolic potential of the microbial community as a whole. This integrated approach allowed for better characterization of the microbial functions responsible for carbon decomposition and a more predictive understanding for how the carbon storage capacity of salt marshes will respond to current and future nitrogen loading.

Methods:

Sample collection & experimental design

We collected sediment along a depth gradient in the tall ecotype of *Spartina alterniflora* at West Creek, a relatively pristine marsh complex located in Plum Island Sound, MA (42.759 N,

70.891 W) that is monitored as part of a long-term experiment called the TIDE project (Deegan et al. 2007). We collected three replicate cores (5 cm diameter, 30 cm deep) within 5 meters of one another and sectioned them under anoxic conditions into shallow (0-5 cm), mid (10-15 cm), and deep (20-25 cm) depths, thus representing a range in OM composition and complexity from newly deposited material to material ranging from 50-100 years in age and found largely below the rooting zone of the dominant vegetation (Wilson et al. 2014, Forbrich et al. 2018).

Briefly, after transporting cores from the field to the lab, we homogenized sediment under anoxic conditions and removed as much live root material as possible. We subsampled homogenized sediment from each depth to characterize parameters from before the start of the experiment (n = 9 "pre-treatment" samples). We then loaded flow through reactors (n =18), each with a volume of 31.81 cm^3, (modified from Pallud & Van Cappellen 2006; Pallud et al. 2007) with homogenized sediment under anoxic conditions, and randomly assigned each reactor a treatment: NO_3^- (n = 9), which consisted of 500 µM $K^{15}NO_3^-$ in 0.2 µm filtered seawater (Cambridge Isotope Laboratories) or unamended (n = 9), which was 0.2 µm filtered seawater meant to represent natural marsh conditions. In both treatments, we bubbled 0.2 µm filtered seawater with nitrogen gas (N_2) until anoxia was reached, which we confirmed with a handheld Hach HQ30D dissolved oxygen meter (Hach Products, Loveland, OH). Subsequently, half of the reactors (n = 9) received the NO_3^- treatment and half received the unamended treatment, both at a targeted flow rate of 0.08 mL min^{-1} using MasterFlex FDA viton tubing (Cole Parmer) under continuously anoxic conditions in a glove bag. Although the top 1-2 mm of sediment at the

surface and adjacent to the roots of marsh vegetation can be oxic, generally oxygen is used almost immediately upon production and the remaining sediment is anoxic. Since we homogenized the top 5 cm for the reactors, the preponderance of the sediment within the core was anoxic, which is why all incubations were performed under anoxic conditions. A more detailed description of the methodology used in this experiment, which lasted for 92 days, can be found in Bulseco et al. (2019).

Metabolism measurements

We collected water samples approximately every 10 days from both the NO_3^- and unamended treatment effluent, as well as each corresponding reservoir influent, to assess biogeochemical processes as a result of microbial activity in each reactor. We measured dissolved inorganic carbon (DIC; $CO_2 + HCO_3 + CO_3^{2-}$) on an Apollo SciTech AS-C3 DIC analyzer, NO_3^- consumption on a Teledyne T200 NOx analyzer (Teledyne API) using chemoluminescent methods (Cox 1980), and ammonium (NH_4^+) and sulfide (HS^-) production on a Shimadzu 1601 spectrophotometer using colorimetric methods as outlined in Solorzano (1969) and Gilboa-Garber (1971), respectively. To assess denitrification, we collected water samples in airtight cut-off volumetric pipettes, preserved them with zinc chloride ($ZnCl_2$), and measured the production of $^{29+30}N_2$ (Nielson et al. 1992) on a membrane inlet mass spectrometer (Kana et al. 1994) connected to a heated (600ºC) copper column to reduce oxygen interference (Eyre et al. 2002, Lunstrum & Aoki 2016). We also measured DNRA following the OX/MIMS methods outlined in Yin et al. (2014). Briefly, we bubbled ~12 mL of sample with helium for 10 minutes

and converted $^{15}NH_4^+$ to $^{29+30}N_2$ using hypobromite iodine. For each biogeochemical measurement, we defined the rate of consumption or production as the difference between the outflow and inflow divided by the flow through reactor volume (31.81 cm^3), corrected by flow rate. We then calculated a cumulative flux by integrating between each measured point throughout the duration of the experiment.

Organic matter composition

We extracted and analyzed lipid biomarker compounds from the sediments at the end of the experiment using a modified method from Bligh & Dyer (1959). To extract total lipids, we mixed approximately 3 g wet sediment with a methanol:dichloromethane:phosphate buffer saline (MeOH:DCM:PBS) mixture (2:1:0.8) and heated to 80ºC for 10 minutes with constant stirring in a microwave-accelerated reaction system (MARS6). We then partitioned samples with a 1:1:0.9 ratio of MeOH:DCM:PBS, removed the organic phase, and concentrated the samples under N_2. To separate each sample into neutral and glycolipids (F1/2) or phospholipids (F3; Guckert et al. 1985), we used a silica gel column and eluted with DCM, acetone, and MeOH, respectively. We dried the F3 (phospholipids) under N_2 and saponified them with 0.5 M sodium hydroxide (NaOH) at 70ºC for 4 hours following Osburn et al. (2011). We then acidified the samples with 3 mL 3N hydrochloric acid (HCl) and extracted 3x with hexane. The phospholipid fraction was methylated by adding acidic methanol (95:5 methanol:HCl) and heating overnight at 70 ºC to form fatty acid methyl esters (FAME). Phospholipid-linked fatty acids (PLFAs) were analyzed with an Agilent 7890 gas chromatograph with an effluent split ~70:30 between a 5975C mass

spectrometer and a flame ionization detector. Peaks were separated on an Agilent DB-5 ms column (60 m, 0.25 mm inner diameter, 0.25 μm film) with methyl heneicosanoate as an internal standard following methods in Spivak and Ossolinski (2016) and references therein. We designated fatty acids (FAs) as A:BωC, where A is the number of carbon atoms, B represents the number of double bonds, and C indicates the position of the double bond relative to the aliphatic end of the molecule as designated by "ω" (Canuel et al. 1995). Individual compounds were assigned to sub-classes representing general microbes (monounsaturated FAs $C_{16:1}$+$C_{17:1}$+$C_{18:1}$+$C_{19:1}$; MUFA), bacteria (iso- and anteiso- branched $C_{13:0}$+$C_{15:0}$+$C_{17:0}$+$C_{19:0}$; BrFA), a combination of algae and microbes (Short chain FAs $C_{12:0}$ + $C_{14:0}$ + $C_{16:0}$; SCFA), and vascular plants (long chain FAs $C_{24:0}$+$C_{26:0}$+$C_{28:0}$+$C_{30:0}$; LCFA) (Perry et al. 1979, Volkman et al. 1989). Each sub-class was then normalized against grams of total organic carbon (TOC) per sample that was measured by elemental analysis.

DNA extraction, library preparation, and sequencing

We extracted genomic DNA from approximately 0.25 g wet sediment from both the pre-treatment sediments (n=9) and treated samples (i.e. NO_3^- and unamended; n=9 each) using the MoBio® PowerSoil DNA Isolation Kit (MoBio Technologies) following manufacturer's instructions, and eluted the DNA into 35 μL of DEPC water. After confirming DNA quality (260/280) and concentration (ng/μL) using a NanoDrop (ThermoFisher Scientific), we sheared 100 ng of DNA to 270 bp fragments in a V2 8-microtube strip run on a Covaris ME220 focused-ultrasonicator at 1000 cycles per burst, 20% duty factor, and 70% peak power for 88 seconds per

sample. We then cleaned the sheared DNA using a 1:1 ratio of Ampure XP purification beads (Beckman Coulter) to sample according to the manufacturers recommendations.

We prepared 27 metagenomic libraries using the NuGEN Ovation Ultralow System V2, performing end repair and barcode ligation with the recommended PCR cycling conditions (25ºC for 30 min and 70ºC for 10 min) and purification methods (Agencourt AMPure XP; Beckman Coulter). We then amplified the final library under the following conditions: 72ºC for 2 min, 95ºC for 3 min, 9 cycles (98ºC for 20 sec, 65ºC for 30 sec, 72ºC for 30 sec), and 72ºC for 1 min, and size-selected the amplification product on a per-sample basis at 390 bp including adaptors using a PippinPrep (Sage Science). After confirming a target insert size of 270 bp on an Agilent 4200 TapeStation (Agilent Technologies), we quantified each library using a KAPA library quantification kit (Roche Sequencing) and performed sequencing on an Illumina NextSeq Hi-Output 2x150 Illumina flow cell (Illumina Inc.) at the Marine Biological Laboratory Keck Facility (Woods Hole, MA).

Sequence analysis and annotation

We joined paired end reads using illumina-utils with a P=0.1, which allows for 1 error in every ten bases, and eliminated read pairs if 66% of bases in the first half of the read contained Q-scores below 30 as recommended in Minoche et al. (2011), resulting in 93% of raw reads being retained after quality filtering (Table S2). Following quality filtering, metagenomic sequencing resulted in 27 (n = 9 for pre-treatment, n = 9 for unamended treatment, and n = 9 for NO_3^- treatment) samples with an average of 2.4×10^7 ($\pm 6.7 \times 10^6$) reads and 43.97% ± 3.26 of

sequences annotated to a known protein per sample (Table S2). We submitted merged reads to the MG-RAST server (Meyer et al. 2008) and performed functional annotation using SEED subsystems (Overbeek et al. 2005; Aziz et al. 2008) with the default of 60% minimum cutoff identity. In this annotation procedure, functions are placed into a subsystem that consists of an abstract functional role. These abstract functional roles are grouped together into larger cellular functions to form categories (Level 1), sub-categories (Level 2), subsystems (Level 3), and roles (Level 4). These subsystems represent different hierarchies of resolution, with Level 1 representing the broadest category and Level 4 representing the specific functional gene annotation. For example, the cytochrome cd1 nitrite reductase gene (*nirS*) would be a Level 4 classification for a gene in the denitrification pathway (Level 3) that is part of nitrogen metabolism (Level 1). For our purposes, we will refer to each SEED subsystem according to its numerical hierarchical level (L1, L2, L3, and L4) throughout the text. All metagenomic data and metadata are publicly available on the MG-RAST website under project no. mgp84173; see Table S2 for unique MG-RAST sample IDs.

Statistical analyses

First, we assessed differences in the biogeochemical fluxes measured from our flow through reactor experiments. To test the hypothesis that addition of NO_3^- would enhance respiration processes, we ran a two-way ANOVA on cumulative DIC production and SO_4^{2-} reduction with treatment and depth as fixed effects. For parameters only detected or measured (NO_3^- reduction and denitrification/DNRA, respectively) in the NO_3^- treatment, we tested for

differences among depths using a one-way ANOVA. To explore differences in PLFAs between treatments, we reduced the dimensionality of the data using a principal components analysis with the 'prcomp' function in R, with centering and scaling set to true (R Core Team), and visualized the results using ggbiplot (Vu 2011). We then compared total PLFA concentration and the relative abundance of BrFA (bacteria), MUFA (plankton + bacteria), and LCFA (plant-derived material) across depths and treatments using a two-way ANOVA. All statistical tests were conducted with an alpha of 0.05 in the R Base package unless otherwise noted (R Core Team, 2013).

Next we tested for differences in our metagenomic data as a function of depth in the sediment, however, prior to testing for differentially abundant functions, we normalized all SEED subsystem annotations by dividing the number of hits to SEED by sequencing depth of the sample and multiplying by 10^6. We examined patterns in metabolic potential by depth in the pre-treatment samples (sediment collected prior to the experiment) by first removing any L3 annotation whose normalized abundance did not occur at least 100 times in any one of the 27 samples. We conducted a one-way ANOVA among shallow, mid, and deep sediments in STAMP (Statistical Analyses of Metagenomic Profiles v. 2.1.3; Parks & Beiko 2010) with a Benjamini-Hochberg correction to minimize false discovery rate (FDR) and visualized the relative abundance of significant subsystems with a heatmap using 'geom_tile' in ggplot2 (Wickham 2016). We then constructed a non-metric multi-dimensional scaling plot and tested for significance by depth and treatment with a permutational multivariate analysis of variance

(PERMANOVA) using the 'adonis' function in the Vegan package (Oksanen et al. 2017; R Core Team, 2013) after testing for homogeneity of dispersion using the 'betadisper' function in phyloseq v.1.22.3 (McMurdie & Holmes 2013).

Next, to investigate differences in metabolic potential between the NO_3^- (n=9) and unamended (n=9) treatments at the end of the experiment, we used a two-sided Welch's t-test with a Benjamini-Hochberg correction in STAMP (Parks & Beiko 2010). We visualized differences in mean proportion of L4 roles and L1 categories between treatments using a scatterplot and extended bar plot, respectively. We chose these sub-systems to look at both the broadest systems-level resolution (L1) and also at the level of the specific protein-coding genes of interest (L4). To further explore differences by treatment, we then selected L3 subsystems within relevant L1 categories based on our hypotheses ("nitrogen metabolism", "sulfur metabolism", "carbohydrates", "metabolism of aromatic compounds", and "respiration") and tested for significance between treatments using a Welch's two-sided t-test with a Benjamini-Hochberg correction in STAMP. We then visualized differences in L3 subsystem abundance by treatment with diverging bar plot. Finally, of the L4 roles that were significantly different between treatments within "nitrogen metabolism" and "sulfur metabolism" L1 categories, we calculated Pearson correlation coefficients between measured rates (DIC production, SO_4^{2-} reduction, NO_3^- reduction, denitrification, and DNRA) and L4 role abundance using the 'cor.test' function in R (R Core Team). We visualized correlation coefficients with a heatmap. Since we determined NO_3^- reduction was negligible in the unamended treatment (Bulseco et al., 2019), we

performed correlations using a cumulative rate of "0" with the assumption that no cryptic NO_3^- cycling was occurring in our anoxic sediments.

Results

Biogeochemical rates:

We observed significant differences in measured biogeochemical rates as a function of both depth and treatment (NO_3^- addition) in our flow through reactor experiments (Fig. 1). The cumulative rates of DIC production ($p<0.001$, $F_{2,14}=48.33$), SO_4^{2-} reduction ($p=0.029$, $F_{2,12}=4.81$), and DNRA ($p<0.001$, $F_{2,6}=27.29$) were all significantly greater in shallow sediments when compared to mid and deep sediments (Fig. 1). However, this pattern was not significant for cumulative NO_3^- reduction ($p=0.156$) or denitrification ($p=0.056$). Consistent with our hypothesis, the addition of NO_3^- significantly affected both DIC production and SO_4^{2-} reduction, with cumulative rates of DIC production being greater in the NO_3^- amended treatments ($p<0.001$, $F_{1,14}=21.73$) and cumulative rates of SO_4^{2-} reduction being greater in the unamended treatments ($p=0.029$, $F_{2,12}=4.81$). NO_3^- reduction rates in the unamended treatment were monitored but negligible. More detailed results on the biogeochemical rates can be found in Bulseco et al. (2019).

Phospholipid-linked fatty acids

The most abundant PLFAs across all samples were $C_{16:0}$, $C_{16:1\omega7}$, iso- and anteiso- $C_{15:0}$, and $_{C18:1\omega9}$ (Fig. S1; Table S1). A PCA indicated a clear separation between NO_3^- and unamended treatments, with 10-Methyl C16:0 (SO_4^{2-} reducers), BrFA (bacteria) and PUFA (microalgae)

driving patterns in the unamended treatment and MUFA (general microbes) and LCFA (plant-derived material) driving patterns in the NO_3^- treatment (Fig. 2a). Total PLFA concentration decreased significantly by depth ($p<0.001$, $F_{2,14} = 22.55$), but showed no difference by treatment ($p=0.379$; Fig. 2b, Fig, S1, Table S1). In contrast, the relative proportion of LCFA (vascular plants) increased significantly with depth (Fig. 2e; $p=0.008$, $F_{2,14}=27.04$) but also demonstrated no pattern by treatment ($p=0.944$). Percent MUFA (microbes) was greater in the NO_3^- treatment ($p=0.018$, $F_{1,14}=7.14$), and this pattern was true across all depths. In contrast, %BrFA (bacteria) was significantly higher in the unamended treatment (Fig. 2c; $p=0.003$, $F_{1,14}=12.79$).

Metagenomic-predicted functions by depth in pre-treatment sediments

A one-way ANOVA revealed several L3 subsystems that were significantly different among depths in the pre-treatment samples (Fig. 3; Table S3). Overall, the majority of functions related to respiration (i.e. terminal cytochrome C oxidases), central carbohydrate metabolism (i.e. dehydrogenase complexes and Enter-Doudoroff pathway), and carbon fixation (i.e. carboxysome) were all greater in shallow sediments. The exceptions were lactate fermentation, glycogen metabolism, acetyl-CoA to Propionyl CoA module, trimethylamine N-oxide reductase, H2:CoM-S-S-HTP oxidoreductase, and anaerobic respiratory reductases, which were greatest in the deepest sediments. The abundance of L3 subsystems within the “aromatic metabolism” were split among depths, with the 4-hydroxyphenylacetic acid catabolic pathway, anaerobic benzoate metabolism, anaerobic toluene and ethylbenzene degradation, central meta-cleavage pathway of aromatic compound degradation, N-heterocyclic aromatic compound degradation, and quinate

degradation exhibiting greatest abundance at the surface. In contrast, aromatic amine catabolism, the carbazole degradation cluster, homogentisate pathway of aromatic compound degradation, n-phenylalkanoic acid degradation, and the core phenylacetl-CoA-catabolic pathway were all most abundant in the deepest sediments. Within the "sulfur metabolism" L1 category, both dimethylsulfoniopropionate (DMSP) breakdown and sulfur oxidation were greatest in the shallow sediments, while SO_4^{2-} reduction-associated complexes were most abundant in the deep sediments. Lastly, L3 subsystems related to NO_3^- and NO_2^- ammonification, denitrification, and ammonia assimilation were all greatest in the shallow sediments. This was in contrast to nitrosative stress and nitrogen fixation, which exhibited greater abundance at depth (Fig. 3; Table S3).

Metagenomic-predicted functions by treatment

When examining all L1 categories with an NMDS (stress = 0.101), there were clear separations along both the primary and secondary axes from sediments at the end of the experiment (Fig. 4a). A PERMANOVA revealed significant differences by treatment (p=0.001, $F_{2,22}$=23.24) and depth (p=0.007, $F_{2,22}$=4.29), but not the interaction of the two (p=0.114). This pattern by treatment was also evident in the 571 L4 roles that deviated considerably from a 1:1 line between NO_3^- and unamended treatments (Fig. 4b). Notable L1 categories enriched in the NO_3^- treatment included nitrogen metabolism and metabolism of aromatic compounds, while L1 categories more abundant in the unamended treatment included carbohydrates and respiration (Fig. 4c).

The addition of NO_3^- fundamentally altered the metabolic potential of these sediments, regardless of depth, with all the patterns described below being statistically significant (Fig. 5, Table S5). The addition of NO_3^- enhanced several L3 subsystems within the "nitrogen metabolism" L1 category, including denitrification, dissimilatory NO_3^- reductase, and NO_3^-/ NO_2^- ammonification; in contrast, nitric oxide synthase and nitrogen fixation were enhanced in the unamended treatment. While both galactosylceramide/sulfatide metabolism and inorganic sulfur assimilation demonstrated greater abundance in the unamended treatment, as expected, sulfur oxidation was greater in the NO_3^- treatment; there was, however, no difference between treatments in SO_4^{2-} reduction-associated complexes. Several pathways within the "carbohydrates" category that involve utilization of sugars (mononsaccharides – Fig. 5i, di- and oligosaccharides – Fig. 5l, polysaccharides – Fig. 5f, and sugar alcohols – Fig. 5e) were enriched in the unamended treatment, with the exception of the serine-glyoxylate cycle, which increased in response to NO_3^-. The abundance of L3 subsystems pertaining to CO_2 fixation (Fig. 5m), such as CO_2 uptake (carboxysome) and the Calvin-Benson cycle, were all considerably higher in the NO_3^- treatment. All L3 subsystems involved in central carbohydrate metabolism (Fig. 5n), with the exception of dihydroxyacetone kinases, were enriched in the NO_3^- treatment, in addition to mixed acid fermentation (Fig. 5k). In contrast, butanediol-related pathways and sugar utilization in fermentative bacteria were enriched in the unamended treatment. Finally, the majority of L3 subsystems related to metabolism of aromatic compounds were more abundant in the unamended

treatment, although the phenylacetyl-CoA catabolic pathway, n-phenylalkanoic acid degradation, and benzoate catabolism increased in response to NO_3^- (Fig. 5c-d).

Correlations between L4 functions and biogeochemical rates

Pearson's correlation coefficients indicated a large degree of correlation between cumulative biogeochemical rates and L4 roles involved in nitrogen and sulfur cycling (Fig. 6; see Table S5-9 for *p*-values and correlation coefficients). Many sulfur-related L4 roles related to sulfur oxidation, such as sulfur oxidation protein, sulfite oxidase, and sulfur oxidation molybdopterin C protein, all exhibited positive correlations with DIC production (Fig. 6b; Table S5) and NO_3^- related process rates (i.e. NO_3^- reduction, denitrification, and DNRA; Tables S6-8). Alkyl hydroperoxide reductase protein C and *DsrM* were signficantly positively correlated with SO_4^{2-} reduction. Both *DsrK* and dissimilatory-type sulfate adenylyltransferase exhibited a positive correlation coefficient when compared with SO_4^- reduction, however the correlation itself was not significant (Fig. 6c; Table S9). Interestingly, the remaining L4 roles related to SO_4^{2-} reduction were not correlated with SO_4^{2-} reduction, but rather, with DIC production, NO_3^- reduction, denitrification, and DNRA (Fig. 6c; Tables S5-8). Several L4 roles related to nitrogen fixation, including nitrogenase (iron-molybdenum cofactor scaffold and assembly protein, nitrogenase (molybdenum-iron) specific transcriptional regulator, and iron-cluster assembly scaffold protein, exhibited a significantly negative relationship with NO_3^- related processes (NO_3^- reduction, denitrification, and DNRA; Fig. 6f; Tables S6-8) and a positive relationship with SO_4^{2-} reduction (Table S9). L4 roles associated with denitrification (cytochrome cd1 NO_2^-

reducatase and nitrous-oxide reductase) and dissimilatory NO_3^- reductase (NO_2^- reductase associated c-type) all showed a positive correlation with denitrification and DNRA, in addition to a negative correlation with SO_4^{2-} reduction (Fig. 6j; Tables S6-9).

Discussion:

Evidence for resource limitation as a function of depth in pre-treatment sediments

Several gradients, which we have diagrammed in Fig. 7, exist that can control the vertical distribution of salt marsh sediment microbial communities, their associated functional potential, and subsequent process rates. Salt marshes in the northeastern US, where this study was conducted, tend to be OM-rich (Morris et al. 2016; Forbrich et al. 2018). The quantity and chemical complexity of this OM is important, because it facilitates most heterotrophic metabolisms by serving as an electron donor. In general, OM at the surface is oxidized at higher rates than OM at depth because of readily available, high-energy-yielding electron acceptors as well as the supply of fresh, bioavailable OM. This results in a decrease in net heterotrophy with depth and an accumulation of less biologically available forms of OM over time and with depth (Middelburg 1989; Hedges et al. 2000).

We observed evidence of down-core changes in the concentration and composition of PLFAs, which represent readily decomposable OM (Fig. 2; Fig. S1; Table S1). Total PLFA concentrations decreased with depth, indicating an overall depletion in easily decomposed OM. Down-core changes in the relative contributions of different PLFA sub-groups suggest that OM composition was differentially affected by decomposition. For instance, the relative

accumulation of LCFA with depth could indicate that the residual OM pool became more resistant to decomposition since lipids in this group ($C_{24:0}$+$C_{26:0}$ +$C_{28:0}$ +$C_{30:0}$) derive from vascular plants and are generally thought to be less reactive (Kolattukudy 1980; Canuel 1997) (Fig. 2E). These down-core changes in the total amount and composition of PLFAs likely reflects a shrinking pool of readily decomposed OM and, potentially, subsequent energy limitation on heterotrophic respiration processes by the resident microbial community.

This gradient of electron donor availability with sediment depth was also evident in the metagenomic data from pre-treatment sediments, where the majority of L3 subsystems within the "carbohydrates" and "respiration" L1 categories were highest in the shallow sediments and decreased with depth (Fig. 3). This suggests that there was greater functional capacity for respiration where OM was more reactive. Many of the L3 subsystems highest in shallow sediments were associated with the fundamental building blocks of carbon metabolism. For example, several L3 subsystems in the TCA cycle, converting pyruvate to CO_2, were significantly higher in the surface sediments than in deep sediments, as were several mechanisms for the formation of pyruvate to feed the TCA cycle, including the glyoxylate bypass and the Entner-Doudoroff pathway. In addition to carbon respiration pathways, multiple L3 subsystems involved in electron transport, such as terminal C oxidases, were also higher at the surface, further supporting our conclusion that the genetic capacity for respiration is highest in the shallow sediments (Fig. 3). This is likely due to a combination of more biologically available organic matter and the limited supply of oxygen provided by diffusion or advection from surface

waters or release from plant roots and is corroborated by the significantly higher DIC production in the shallow compared to the deep sediments during the experimental incubation (Fig. 1). L3 subsystems related to carbohydrate utilization were also more abundant in shallow sediments, including cellusomes, which facilitate the anaerobic decomposition of cellulose (Bule et al. 2018) and the metabolism of simple monosaccharides, such as xylose and mannose that are known to be readily leached from salt marsh vegetation (Pakulski 1986). By contrast, L3 subsystems indicative of resource limitation (i.e. less bioavailable OM), including functions associated with anaerobic respiration and fermentation (glycolysis, acetone butanol, and ethanol fermentation) were enriched at depth. Similarly, L3 subsystems involved in glycogen metabolism, a strategy often employed to cope with episodic starvation (Wilson et al. 2010), were also enriched at depth.

The availability of electron acceptors is another factor that can control subsurface microbial communities and biogeochemical functions. Microbes preferentially reduce electron acceptors that yield the most energy (greater Gibb's free energy; ΔG^o), resulting in a predictable sequence of metabolic processes (Froelich et al. 1979; Thamdrup et al. 1994). In salt marshes, oxygen is rapidly consumed within the first few millimeters of the surface (Teal & Kanwisher 1961), leaving the majority of microbial metabolic processes to rely on anaerobic metabolisms, such as NO_3^- reduction, SO_4^{2-} reduction, and fermentation. Our metagenomic data from pre-treatment sediments exhibited patterns that closely mimic this idealized sequence of metabolic processes based on thermodynamic theory. In shallow sediments, energetically favorable

processes such as denitrification, were more abundant than at depth. In contrast, less thermodynamically favorable processes, such as SO_4^{2-} reduction, fermentation (Canfield et al. 2005), and functions related to anaerobic respiratory reductases, became more abundant in deep sediments. Thus, the functional potential we observed in the microbial community reflect the ecological gradients that occur along a sediment profile, both in OM complexity and electron acceptor availability.

Separate from respiratory processes, we also found that the abundance of the nitrogen fixation L3 subsystem increased with depth (Fig. 3). This could be due to several reasons. Since NO_3^- is typically a limiting resource in many coastal systems (Ryther & Dunstan 1971), nitrogen fixation is one way the community can overcome this resource limitation by reducing atmospheric nitrogen and converting it into ammonia and other nitrogenous forms (Jones 1974; Postgate 1982). However, ammonium concentrations in salt marsh sediments are generally high, which seems to contradict this hypothesis. In salt marshes SO_4^{2-} reducers and fermenters such as *Clostridia* can also contribute significantly to nitrogen fixation under anaerobic conditions (Carpenter et al. 1978; Dicker & Smith 1980; Gandy & Yoch 1988). There is also evidence for increased occurrence of nitrogen fixation where OM is more processed and NO_3^- is limiting. Fulweiler et al. (2013) observed that increases in *nifH* expression coincided with decreases in denitrification as deposited OM aged over time. Lastly, increased abundance of nitrogen fixation genes at depth could also be a result of electron dumping, where organisms use nitrogen fixation as a way to regulate their intracellular redox state (McKinlay & Harwood 2010; Bombar et al.

2016). Overall, although we cannot definitively identify the main driver of the increased metabolic capacity for nitrogen fixation at depth, one of the potential explanations for the pattern we observed can be attributed to resource limitation. Whether this pattern is due to changes in OM complexity, decreased availability of NO_3^-, or the subsequent increase in nitrogen-fixing SO_4^{2-} reducers and fermenters, remains unclear.

Resource limitation in the unamended treatment

At the end of the experiment, the microbial community from the unamended treatment, regardless of the depth from which the sediment was collected, exhibited properties similar to that of pre-treatment sediments from the deepest depth (Fig. 7). Increased abundance of L3 subsystems related to nitrogen fixation, SO_4^{2-} reduction, fermentation, and anaerobic respiratory reductases all suggest resource limitation (Fig. 7). By the end of the 92-day experiment, the microbial community in the unamended treatment, where SO_4^{2-} was the dominant electron acceptor, appeared thermodynamically constrained and only able to access certain forms of OM; the less bioavailable OM forms therefore accumulated over time, resulting in decreased DIC production (Fig. 1; Bulseco et al., 2019). Our metagenomic data provide evidence for these patterns. We found that, while microbes in the unamended treatment had some capacity to degrade aromatic carbon typical of salt marsh sediments, they also exhibited properties of using simple, low complexity sugars (Fig. 5f, 5f, and 5o). This suggests that the heterotrophic community was energetically constrained to oxidizing simple forms of OM through less efficient

metabolisms that tend to dominate under energy-deprived conditions (Westrich & Berner 1984; Middelburg 1989; Burdige 2007).

Several L3 subsystems involved in less efficient metabolisms, such as fermentation, were higher in the unamended treatment. This process shunts electrons among organic compounds rather than the electron transport chain, resulting in very low energy production. As an outcome, several organic acids and alcohols are produced that other microbial groups can subsequently use to fuel respiration (Morris et al. 2013; Hug & Co 2018). In our metagenomic data, we found most notably that acetoin butanediol metabolism, acetone butanol ethanol synthesis, butanol biosynthesis, and acetyl-CoA fermentation to butyrate were enriched in the unamended treatment (Fig. 5k). Butanol biosynthesis, in particular, is a strictly anaerobic process using plant material as a carbon source (McNeil & Kristiansen 1986).

Another line of evidence for energy limitation in the unamended treatment was the presence of L3 functions involved in methanogenesis, including increased abundance of H2:COM-S-S-HTP oxidoreductase (Fig. 5). Enzyme encoding genes within this subsystem act on sulfur groups of electron donors and are mainly found in methanogenic archaea (Deppenmeier et al. 1991; Setzke et al. 1994). This process, which either uses carbon (typically acetic acid or carbon dioxide) or other small organic compounds, produces methane and typically only becomes important when all other electron acceptors are depleted (Kunkel et al. 1997; Yan et al. 2018). Similar to the deepest pre-treatment sediments, the abundance of glycogen metabolism was enriched at the end of the experiment in the unamended treatment, suggesting a

greater capacity for energy reserves to cope with temporary conditions of limitation in the environment (Wilson et al. 2010). Interestingly, L3 subsystems related to SO_4^{2-} reduction were not enriched, however this could simply be due to the fact that this metabolism was supported across both treatments.

Similar to the deep pre-treatment sediments, nitrogen fixation was also promoted in the unamended treatment (Fig. 5, 7). In a different study that sequenced the 16S rRNA genes from this experiment, several taxa belonging to groups known to reduce SO_4^- increased in abundance in the unamended treatment (i.e. Desulfobacterales and Desulfarculales; Bahr et al. 2005; Bulseco et al., 2019). Further, several L4 functions related to nitrogen fixation (*NifN, NifE, NifU, and NifA*; Gussin et al. 1986; Kuypers et al. 2018) were positively correlated with SO_4^{2-} reduction and negatively correlated with NO_3^- reduction-related pathways, suggesting that the promotion of SO_4^- reducers (and, in contrast, their inhibition by excess supply of NO_3^- in the enhanced treatment) is important in enhancing the functional potential for nitrogen fixation.

Nitrate-enhanced respiration

The addition of NO_3^- appeared to relieve the microbial community of the resource limitation observed in the unamended and the pre-treatment deep sediments, as demonstrated by a general increase in L3 subsystems involved in respiration and electron transport (Fig. 5, 7). Some examples of these groups include respiratory complex I, which translocates protons across the bacterial membrane and contributes to the synthesis of ATP (Wilkstrom & Hummer 2012), as well as terminal cytochrome C oxidases that shuttle electrons to and from macromolecular

complexes within the membrane (Chen & Strous 2013). The observed increase in respiration-related functions was further supported by the increase of L3 subsystems within the 'central carbohydrate metabolism' subcategory that all contribute to the production of ATP, including glycolate-glyoxylate interconversions, pyruvate metabolisms, ethylmalonyl-CoA pathway of C2 assimilation, and glyoxylate bypass (Fig. 5n; Erb et al. 2007; Peyraud et al. 2009; Petushkova et al. 2018). Increased abundance of the Entner-Doudoroff pathway, which converts glucose to pyruvate (Conway 1992), and dehydrogenase complexes, which decarboxylates pyruvate into acetyl-CoA to fuel cellular respiration (de Kok et al. 1998), provide additional evidence for the enhancement of respiration in the NO_3^- treatment. These metagenomic data agree with increased DIC production we observed in response to NO_3^- (Fig. 1).

Several L3 functions related to nitrogen metabolism in particular increased in response to NO_3^- (Fig. 4C), likely contributing to the overall increase in respiration (Fig. 1). Because NO_3^- is typically limiting in coastal systems (Ryther & Dunstan 1971) and is a more energetically favorable electron acceptor than SO_4^{2-} (Canfield et al. 2005), it is not surprising that the microbial community shifted towards functions that effectively utilize NO_3^-. For example, L3 subsystems related to denitrification, dissimilatory NO_3^- reductase, and NO_3^- and NO_2^- ammonification all significantly increased in the NO_3^- treatment (Fig. 5, 7). Enzyme encoding genes within these L3 subsystems, including cytochrome cd1 NO_2^- reductase and nitrous-oxide reductase (denitrification; Fig. 6j), NO_2^- reductase associated c-type cytochrome NirN (dissimilatory NO_3^- reductase; Fig. 6i), NO_3^-/NO_2^- transporter, respiratory NO_3^- reductase alpha

chain, and respiratory NO_3^- reductase alpha chain, among others (NO_3^-/ NO_2^- ammonification; Fig. 6h) all exhibited significantly positive correlations with NO_3^- reduction, denitrification, and DNRA (Tables S6-8). This provides further evidence that functions inferred by the metagenomic data corroborate measured biogeochemical rates.

Increased abundance of microbes could also explain the enhanced respiration we observed in both the rate measurements (Fig. 1) and metagenomic data (Fig. 5) associated with the NO_3^- enriched sediments. Although we did not perform cell counts for these samples, if microbe abundances were higher in the NO_3^- treatment, we would expect to see an increase in L3 and L4 functions related to ammonia uptake and transport in response to NO_3^- (Jansson 1958); however, we actually observed the opposite. Ammonia assimilation genes were significantly greater in the unamended treatment (Fig. 5) and there was no significant correlation between ammonia transport genes and any measured biogeochemical rates (Fig. 6k). Further, our PLFA data show that BrFA, which are bacteria-specific biomarkers (Perry et al. 1979; Volkman et al. 1989), exhibited significantly higher relative abundance in the unamended treatment (Fig. 2; Table S1). These lines of evidence suggest that there were not higher abundances of microbes in the NO_3^- treatment and therefore that NO_3^- stimulates respiration rather than enhancing microbial growth.

Finally, subsystems related to nitrogen fixation were less abundant in the NO_3^- treatment (Fig. 5) and were negatively correlated with NO_3^- related processes, presumably due to the release of N limitation within the system. Further, 16S rRNA gene data from this experiment

demonstrated decreased alpha diversity of the overall community at the expense of SO_4^{2-} reducers, which also may hinder the metabolic capacity for nitrogen fixation (Bulseco et al., 2019). Although we did not explicitly measure nitrogen fixation in our experiment, similar patterns have been observed in prior studies, where decreased rates of nitrogen fixation occurred in response to nitrogen inputs (Moseman-Valtierra et al. 2010; Fulweiler et al. 2013).

Increased respiration of organic matter has cascading effects

When NO_3^- was no longer limiting, a series of cascading effects seems to have altered the overall function of the microbial community leading to enhanced respiration and OM oxidation. Increased rates of respiration, particularly denitrification and DNRA, coincided with greater abundance of L3 subsystems associated with the ability to break down complex forms of OM (Fig. 5c; e.g. the phenyl-CoA catabolic pathway, benzoate transport and degradation cluster, and n-phenylalkanoic acid degradation subsystems). The enhancement of these groups provides evidence that microbes under a NO_3^- rich environment can break down complex carbohydrates into simpler forms. Several L3 subsystems within the glycolate-glyoxylate interconversions subsystem, including various reductases, dehydrogenases, and the glyoxylate cycle, as well as the ethylamlonyl-CoA pathway, were also enriched in response to NO_3^- (Fig. 5n). Many of these pathways provide mechanisms for survival on simple one- and two-carbon compounds, including methanol (Petushkova et al. 2018; Schneider et al. 2012). For example, the glyoxylate cycle provides a shunt to the more typical TCA cycle, allowing biosynthesis from less complex forms of carbon. Their presence suggests a syntrophic community of microbes that are able to use the

simple carbohydrates liberated via decomposition of more complex carbohydrates that is enhanced under high NO_3^- supply.

There is additional evidence for such syntrophic relationships, with other simple compounds produced from these processes being used by other microbial groups. For example, mixed acid fermentation, where glucose is fermented into either acetate, ethanol, lactate, succinate, or formate (Müller 2001), was the only fermentation-related process enriched in the NO_3^- treatment, and may have been facilitated by the production of these simple carbon compounds formed as a result of complex carbohydrate decomposition (Fig. 5k). Kearns et al. (2016) found that SO_4^{2-} reducers belonging to the order Desulfobacterales became more active in response to NO_3^- enrichment in salt marsh sediments, and attributed this pattern to their ability to more quickly respond to environmental perturbations (Strittmeyer et al. 2009). However, another explanation could be that NO_3^- enrichment promoted the decomposition of more complex forms of carbon into simpler ones, subsequently making OM more accessible to other microbial groups that would otherwise be unable to utilize it, such as sulfate reducers (Bulseco et al., 2019). This cascading effect on the microbial community by increasing biologically accessible OM to several microbial groups may potentially decrease salt marsh carbon storage capacity.

One pattern we observed, however, contrasts with this, and that is the greater prevalence of subsystems related to carbon dioxide fixation in response to NO_3^-. Instead of depleting the capacity for carbon storage, carbon fixation resulting from electron shuttling between tightly coupled metabolisms may actually offset some of this carbon loss. There are several mechanisms

that could be driving increased carbon fixation. First, the abundance of sulfur oxidation related L3 subsystems within the 'sulfur metabolism' L1 category increased in the NO_3^- treatment (Fig. 5) and was positively correlated with NO_3^- reduction-related processes (Fig. 6b). This chemoautotrophic process that oxidizes reduced sulfur can be coupled to the reduction of NO_3^- (Burgin & Hamilton 2007; Giblin et al. 2013; Thomas et al. 2014) and can occur either through the process of DNRA (Brunet and Garcia-Gil 1996) or denitrification (e.g. Hannig et al. 2007; Hietanen et al. 2012; Dalsgaard et al. 2013). We also found some evidence for increased abundance of the methanogenesis pathway in the NO_3^- treatment (Fig. 5g), which is counter to the dogma that this process only occurs as a last resort due to its low energetic capacity and/or in the absence of other inhibiting processes (Roy & Conrad 1999). Methanogenesis is, however, a reversible process (Hallam et al. 2004) and we could instead be observing evidence of anaerobic methane oxidation (AOM) linked to NO_3^- (NAMO; Raghoebarsing et al, 2006; Haroon et al. 2013) or SO_4^{2-} reduction (Knittel & Boetius 2009; Thauer 2011). Enhanced AOM would result in the oxidation of methane in conjunction with carbon fixation, potentially contributing to carbon burial and sequestration. Overall, increased abundance of L3 subsystems related to carbon fixation suggest that, along with increased respiration, there is also evidence for processes that reverse at least some of this carbon depletion.

Conclusions

We conducted a controlled flow through experiment and measured biogeochemical rates in conjunction with metagenomic sequencing to explicitly test whether NO_3^- increased the

functional potential for respiration of OM from salt marsh sediments. We found that microbes in the unamended treatment, under conditions typical of salt marsh sediments, demonstrated functional potential associated with surviving in low energy (electron donor availability) and thermodynamically-constrained (electron acceptor availability) environments through enhancement in L3 subsystems involved in nitrogen fixation, SO_4^{2-} reduction, fermentation, and anaerobic respiratory reductases at depth (Fig. 7). With the addition of NO_3^-, however, several respiration-related processes such as denitrification, respiratory complex I, and terminal cytochrome C were enhanced, regardless of depth. We hypothesize this response was a result of alleviating the limitation of a more energetically favorable electron acceptor. Once NO_3^- was no longer limiting, we also observed a cascade of alterations to the overall function of the microbial community, including the degradation of complex carbon compounds and enhanced CO_2 fixation through increases in L3 subsystems related to sulfur oxidation, carboxysomes, and the Calvin-Benson cycle (Fig. 7). Most importantly, the controlled experimental approach taken here revealed that measured process rates coincided with detected shifts in metabolic potential. These results contribute towards a more refined and predictive understanding of microbially-mediated biogeochemical cycles in a rapidly changing world.

Acknowledgements

We thank researchers of the TIDE project (NSF OCE0924287, OCE0923689, DEB0213767, DEB1354494, and OCE 1353140) for maintenance of the long-term nutrient enrichment experiment, researchers of the Plum Island Ecosystems LTER (NSF OCE 0423565, 1058747,

1637630), as well as Kelsey Gosselin, who assisted with PLFA analyses. This work was funded by an NSF CAREER Award to JLB (DEB1350491), a Woods Hole Oceanographic Sea Grant award to AEG, JJV, and GTB (Project No. NA140AR4170074 Project R/M-65s), an NSF DDIG award to JLB and ABM (Award No. 1701748), and a Woods Hole Sea Grant (NA18OAR4170104) and NOAA NSC (3004701234) awards to ACS and a NSF DEB award (DEB1655552) to Joseph Vallino and Julie Huber. Additional support was provided by a Ford Foundation pre-doctoral fellowship award to ABM. All sequence data from this study is available on the MG-RAST server under Project no. mgp84173 with associated metadata stored on the Plum Island LTER website. Equipment purchased with funds from the NSF FMSL program (DBI 1722553 to Northeastern University) were used to generate data for this manuscript. Views expressed here are those of the authors and do not necessarily reflect the views of NOAA or any of is sub-agencies.

References

Aziz, R.K. and others. 2008. The RAST Server: rapid annotations using subsystems technology. BMC Genomics 9: 1–15, doi: 10.1186/1471-2164-9-75

Bahr, M., Crump, B.C., Klepac-Ceraj, V., Sogin, M.L., and J.E. Hobbie. 2005. Molecular characterization of sulfate-reducing bacteria in a New England salt marsh. Environ. Microbiol. 7: 1175-1185, doi: 10.1111/j.1462-2920.2005.00796.x

Barbier, E. B., S.D. Hacker, C. Kennedy, E.W. Koch, A.C. Stier, and B.R. Silliman. 2011. The value of estuarine and coastal ecosystem services. Ecol. Monogr. 81: 169-193, doi: 10.1890/10-1510.1

Bier, R. L., and others. 2015. Linking microbial community structure and microbial processes: an empirical and conceptual overview. FEMS Microbiol. Ecol. 91: fiv113, doi: 10.1093/femsec/fiv113

Bligh, E.G. and W. J. Dyer. 1959. A rapid method of total lipid extraction and purification. Can. J. Biochem. Physiol. 37: 911-917, doi:10.1139/o59-099

Bombar, D., R.W. Paerl, and L. Riemann. 2016. Marine non-cyanobacterial diazotrophs: moving beyond molecular detection. Trends Microbiol. 24: 916-927, doi: 10.1016/j.tim.2016.07.002

Brunet, R. C., and L. J. Garcia-Gil. 1996. Sulfide-induced dissimilatory nitrate reduction to ammonia in anaerobic freshwater sediments. FEMS Microbiol. Ecol. 21: 131–138, doi:10.1016/0168-6496(96)00051-7

Bulseco, A., A. Giblin, J. Tucker, A.E. Murphy, J. Sanderman, K. Hiller, J.L. Bowen. 2019. Nitrate addition stimulates microbial decomposition of organic matter in salt marsh sediments. Glob. Change Biol.

Bule, P., V.M. Pires, C.M. Fontes, and V. D. Alves. 2018. Cellulosome assembly: paradigms are meant to be broken! Curr. Opin. Struct. Biol. 49: 154–161. doi:10.1016/j.sbi.2018.03.012

Burdige, D.J. 2007. Preservation of organic matter in marine sediments: Controls, mechanisms, and an imbalance in sediment organic carbon budgets? Chem. Rev. 107: 467–485, doi:10.1021/cr050347q

Burgin, A. J., and S. K. Hamilton. 2007. Have we overemphasized the role of denitrification in aquatic ecosystems? A review of nitrate removal pathways. Front. Ecol. Environ. 5: 89–96. doi:10.1890/1540-9295(2007)5[89:HWOTRO]2.0.CO;2

Canfield, D.E., B. Thamdrup, and E. Kristensen. 2005. Aquatic Geomicrobiology. Elsevier Academic Press.

Canuel, E. A., J. E. Cloern, D. B. Ringelberg, J. B. Guckert, and G. H. Rau. 1995. Molecular and isotopic tracers used to examine sources of organic matter and its incorporation into the food webs of San Francisco Bay. Limnol. Oceanogr. 40: 67–81. doi:10.4319/lo.1995.40.1.0067

Canuel, E. A., K. H. Freeman, and S. G. Wakeham. 1997. Isotopic compositions of lipid biomarker compounds in estuarine plants and surface sediments. Limnol. Oceanogr.42: 1570-1583, doi:10.4319/lo.1997.42.7.1570

Carpenter, E.J., C.D.Van Raalte, and I. Valiela I .1978. Nitrogen fixation by algae in a Massachusetts salt marsh. Limnol. Oceanogr. 23: 318 –327, doi: 10.4319/lo.1978.23.2.0318

Chen, J. and M. Strous. 2013. Denitrification and aerobic respiration, hybrid electron transport chains and co-evolution. Biochim. Biophys. Acta 1827: 136-44, doi: 10.1016/j.bbabio.2012.10.002

Conway, T. 1992. The Entner-Doudoroff pathway: history, physiology and molecular biology. FEMS Microbiol. Lett. 103: 1–28. doi:10.1111/j.1574-6968.1992.tb05822.x

Cox, R.D. 1980. Determination of nitrate and nitrite at the parts per billion level by chemiluminescence. Anal. Chem. 52: 332-335, doi: 10.1021/ac50052a028

Dalsgaard, T., L. De Brabandere and P.O. Hall. 2013. Denitrification in the water column of the central Baltic Sea. Geochim. Cosmochim. Acta, 106: 247-260, doi: 10.1016/j.gca.2012.12.038

Deegan, L.A., J.L. Bowen, D. Drake, J.W. Fleeger, C.T. Friedrichs, K.A. Galván, J.E. Hobbie, and C. Hopkinson. 2007. Susceptibility of salt marshes to nutrient enrichment and predation removal. Ecol. Appl. 17:42–63, doi: 10.1890/06-0452.1

de Kok, A., A. F. Hengeveld, A. Martin, and A. H. Westphal. 1998. The pyruvate dehydrogenase multi-enzyme complex from Gram-negative bacteria. Biochim. Biophys. Acta, Protein Struct. Mol. Enzymol. 1385: 353–366, doi:10.1016/S0167-4838(98)00079-X

Deppenmeier, U., M. Blaut, and G. Gottschalk, G. 1991. H 2: heterodisulfide oxidoreductase, a second energy-conserving system in the methanogenic strain Gö1. Arch. Microbiol. 155: 272-277, doi: 10.1007/BF00252211

Dicker, H. J., and D.W. Smith. 1980. Acetylene reduction (nitrogen fixation) in a Delaware, USA salt marsh. Mar. Biol. 57: 241-250, doi: 10.1007/BF00387567

Erb, T. J., I. A. Berg, V. Brecht, M. Muller, G. Fuchs, and B. E. Alber. 2007. Synthesis of C5-dicarboxylic acids from C2-units involving crotonyl-CoA carboxylase/reductase: The ethylmalonyl-CoA pathway. Proc. Natl. Acad. Sci. U.S.A. 104: 10631–10636, doi:10.1073/pnas.0702791104

Eyre, B.D., S. Rysgaard, T. Dalsgaard, and P.B. Christensen. 2002. Comparison of isotope pairing and N2:Ar methods for measuring sediment denitrification – assumption, modifications, and implications. Estuaries 25: 1077-1087, doi: 10.1007/BF02692205

Falkowski, P. G., T. Fenchel, and E. F. Delong. 2008. The microbial engines that drive Earth's biogeochemical cycles. Science 320: 1034–1039, doi:10.1126/science.1153213

Forbrich, I., A.E. Giblin, and C.S. Hopkinson. 2018. Constraining marsh carbon budgets using long-term C burial and contemporary atmospheric CO2 fluxes. J. Geophys. Res. Biogeosci. 123: 867-878, doi: 10.1002/2017JG004336

Froelich, P., G. Klinkhammer, M. Bender, N. Luedtke, G. Heath, D. Cullen, and P. Dauphin. 1979. Early oxidation of organic matter in pelagic sediments of the eastern equatorial Atlantic: suboxic diagenesis. Geochim. Cosmochim. Acta 43: 1075–1090, doi: 10.1016/0016-7037(79)90095-4

Fulweiler, R. W., S. M. Brown, S.W. Nixon, and B.D. Jenkins. 2013. Evidence and a conceptual model for the co-occurrence of nitrogen fixation and denitrification in heterotrophic marine sediments. Mar. Ecol. Progr. Ser. 482: 57-68, doi: 10.3354/meps10240

Galloway, J.N., A.M. Leach, J.W. Erisman, and A. Bleeker. 2017. Nitrogen: the historical progression from ignorance to knowledge with a view to future solutions. Soil. Res. 55: 417–424, doi: 10.1071/SR16334

Gandy, E. L., and D.C. Yoch.1988. Relationship between nitrogen-fixing sulfate reducers and fermenters in salt marsh sediments and roots of Spartina alterniflora. Appl. Environ. Microbiol. 54: 2031-2036.

Giblin, A., C. Tobias, B. Song, N. Weston, G. Banta, and V. Rivera-Monroy. 2013. The importance of dissimilatory nitrate reduction to ammonium (DNRA) in the nitrogen cycle of coastal ecosystems. Oceanography 26: 124–131, doi:10.5670/oceanog.2013.54

Gilboa-Garber, N. 1971. Direct spectrophotometric determination of inorganic sulfide in biological materials and in other complex mixtures. Anal. Biochem. 43: 129–133, doi: 10.1016/0003-2697(71)90116-3

Graham, E. B., and others. 2016. Microbes as engines of ecosystem function: when does community structure enhance predictions of ecosystem processes? Front. Microbiol. 7: 214, doi:10.3389/fmicb.2016.00214

Graves, C.J., E.J. Makrides, V.T. Schmidt, A.E. Giblin, Z.G. Cardon, and D.M. Rand. 2016. Functional responses of salt marsh microbial communities to long-term nutrient enrichment. Appl. Environ. Microbiol. 82: 2862–2871, doi:10.1128/AEM.03990-15

Guckert, J.B., C.P. Antworth, P.D. Nichols, and D.C. White. 1985. Phospholipid, ester-linked fatty acid profiles as reproducible assays for changes in prokaryotic community structure of estuarine sediments. FEMS Microbiol. Lett. 31: 147–158.

Gussin, G. N., C. W. Ronson, and F. M. Ausubel. 1986. Regulation of nitrogen fixation genes. Annual Review of Genetics, 20: 567-591, doi: 10.1146/annurev.ge.20.120186.003031

Hallam, S.J., N. Putnam, C.M. Preson, J.C. Detter, D. Rokhsar, P.M. Richardson, and E.F. DeLong. 2004. Reverse methanogenesis: Testing the hypothesis with environmental genomics. Science 305: 1457–1462, doi: 10.1126/science.1100025

Hannig, M., G. Lavik, M.M.M. Kuypers, D. Woebken, W. Martens-Habbena, and K. Jürgens. 2007. Shift from denitrification to anammox after inflow events in the central Baltic Sea. Limnol. Oceanogr. 52: 1336-1345, doi: 10.4319/lo.2007.52.4.1336

Haroon, M. F., S. Hu, Y. Shi, M. Imelfort, J. Keller, P. Hugenholtz, Z. Yuan, and G. W. Tyson. 2013. Anaerobic oxidation of methane coupled to nitrate reduction in a novel archaeal lineage. Nature 500: 567–570, doi:10.1038/nature12375

Hedges, J. I., and others. 2000. The molecularly uncharacterized component of nonliving organic matter in natural environments. Org. Geochem. 31: 945–958, doi: 10.1016/S0146-6380(00)00096-6

Hietanen, S., H. Jäntti, C. Buizert, K. Jürgens, M. Labrenz, M. Voss, and J. Kuparinen. 2012. Hypoxia and nitrogen processing in the Baltic Sea water column. Limnol. Oceanogr. 57: 325-337, doi: 10.4319/lo.2012.57.1.0325

Himes-Cornell, A., L. Pendleton, and P. Atiyah. 2018. Valuing ecosystem services from blue forests: A systematic review of the valuation of salt marshes, sea grass beds and mangrove forests. Ecosystem services 30: 36-48, doi: 10.1016/j.ecoser.2018.01.006

Hug, L.A. and R. Co. 2018. It takes a village: microbial communities thrive through interactions and metabolic handoffs. MSystems, 3: e00152-17, doi: 10.1128/mSystems.00152-17

Jansson, S.L. 1958. Tracer studies on nitrogen transformations in soil with special attention to mineralization immobilization relationship. Lantbrukshoegsk. Ann. 24: 101-361

Jones, K., 1974. Nitrogen fixation in a salt marsh. J. Ecol. 62:553-565.

Jones, S. E. and J. T. Lennon. 2010. Dormancy contributes to the maintenance of microbial diversity. Proc. Natl. Acad. Sci. 107: 5881–5886, doi:10.1073/pnas.0912765107

Kana, T. M., C. Darkangelo, M. D. Hunt, J. B. Oldham, G. E. Bennett, and J. C. Cornwell. 1994. Membrane inlet mass spectrometer for rapid high-precision determination of N2, O2, and Ar in environmental water samples. Anal. Chem. 66: 4166–4170, doi:10.1021/ac00095a009

Kearns, P.J., J.H. Angell, E. Howard, L.A. Deegan, R.H. Stanley, and J.L. Bowen. 2016. Nutrient enrichment induces high rates of dormancy and decreases diversity of active bacterial taxa. Nat. Commun. 7: 12881, doi: 10.1038/ncomms12881

Kearns, P. J., A. N. Bulseco-McKim, H. Hoyt, J.H. Angell, and J.L. Bowen. 2018. Nutrient enrichment alters salt marsh fungal communities and promotes putative fungal denitrifiers. Microb. Ecol. 77: 358-369, doi: 10.1007/s00248-018-1223-z

Knelman, J. E. and D. R. Nemergut. 2014. Changes in community assembly may shift the relationship between biodiversity and ecosystem function. Front. Microbiol. 5: 424, doi:10.3389/fmicb.2014.00424

Knittel, K., and A. Boetius. 2009. Anaerobic oxidation of methane: Progress with an unknown process. Annu. Rev. Microbiol. 63: 311–334, doi: 10.1146/annurev.micro.61.080706.093130

Koop-Jakobsen, K. and A.E. Giblin. 2010. The effect of increased nitrate loading on nitrate reduction via denitrification and DNRA in salt marsh sediments. Limnol. Oceanogr. 55: 789–802, doi: 10.4319/lo.2010.55.2.0789

Kolattukudy, P. E. 1980. Biopolyester membranes of plants: cutin and suberin. Science 208: 990-1000, doi:10.1126/science.208.4447.990

Kunkel, A., M. Vaupel, S. Heim, R. K. Thauer, and R. Hedderich. 1997. Heterodisulfide Reductase from Methanol-Grown Cells of Methanosarcina Barkeri is not a Flavoenzyme. European Journal of Biochemistry 244: 226–234, doi:10.1111/j.1432-1033.1997.00226.x

Kuypers, M.M.M., H.K. Marchant, and B. Kartal. 2018. The microbial-nitrogen network. Nat. Rev. Microbiol. 16: 263-276, doi: 10.1038/nrmicro.2018.9

Lennon, J. T. and S. E. Jones. 2011. Microbial seed banks: the ecological and evolutionary implications of dormancy. Nat. Rev. Microbiol. 9: 119–130, doi:10.1038/nrmicro2504

Lozupone, C.A. and R. Knight. 2007. Global patterns in bacterial diversity. Proc. Natl. Acad. Sci. 104: 11436-11440, doi: 10.1073/pnas.0611525104

Lunstrum, A., and L.R. Aoki. 2016. Oxygen interference with membrane inlet mass spectrometry may overestimate denitrification rates calculated with the isotope pairing technique. Limnol. Oceanogr.:Methods 14: 425-431, doi: 10.1002/lom3.10101

McKinlay, J. B., and C.S. Harwood. 2010. Carbon dioxide fixation as a central redox cofactor recycling mechanism in bacteria. Proc. Nat. Acad. Sci. U.S.A. 107: 11669-11675, doi: 10.1073/pnas.1006175107

Mcleod E., G.L. Chmura, S. Bouillon, R. Salm, M. Björk, C.M. Duarte, C.E. Lovelock, W.H. Schlesinger, and B.R. Silliman. 2011. A blueprint for blue carbon: toward an improved understanding of the role of vegetated coastal habitats in sequestering CO2. Front. Ecol. Environ. 9:552–560, doi: 10.1890/110004

McMurdie, P.J. and S. Holmes. 2013. Phyloseq: an R package for reproducible interactive analysis and graphics of microbiome census data. PloS One. 8: e61217, doi:10.1371/journal.pone.0061217

McNeil, B. and B. Kristiansen. 1986. The acetone butanol fermentation. Adv. Appl. Microbiol. 31: 61-92, doi: 10.1016/S0065-2164(08)70439-8

Mendelssohn, I.A. and J.T. Morris. 2000. Ecophysiological controls on the growth of Spartina alterniflora, pp. 59-80. In: Concepts and Controversies in Tidal Marsh Ecology. N.P. Weinstein and D.A. Kreeger [eds.], Kluwer Academic Publishers

Meyer, F. D., and others. 2008. The metagenomics RAST server—a public resource for the automatic phylo- genetic and functional analysis of metagenomes. BMC Bioinf. 9: 386, doi: 10.1186/1471-2105-9-386

Middelburg, J. 1989. A simple rate model for organic matter decomposition in marine sediments. Geochim. Cosmochim. Acta 53: 1577–1581, doi: 10.1007/s10499-012-9533-5, doi: 10.1016/0016-7037(89)90239-1

Minoche, A.E., J.C. Dohm, and H. Himmelbauer. 2011. Evaluation of genomic high-throughput sequencing data generated on Illumina HiSeq and Genome Analyzer systems. Genome Biol. 12:R112, doi: 10.1186/gb-2011-12-11-r112

Morales, S. E., and W.E. Holben. 2011. Linking bacterial identities and ecosystem processes: can 'omic' analyses be more than the sum of their parts? FEMS Microbiol. Ecol. 75: 2-16, doi: 10.1111/j.1574-6941.2010.00938.x

Morris, B. E. L., R. Henneberger, H. Huber, and C. Moissl-Eichinger. 2013. Microbial syntrophy: interaction for the common good. FEMS Microbiology Reviews 37: 384–406, doi:10.1111/1574-6976.12019

Morris, J.T. and others. 2016. Contributions of organic and inorganic matter to sediment volume and accretion in tidal wetlands at steady state. Earth's Future. 4: 110–121, doi: 10.1002/2015EF000334

Moseman-Valtierra, S. M., K. Armaiz-Nolla, and L.A. Levin .2010. Wetland response to sedimentation and nitrogen loading: diversification and inhibition of nitrogen-fixing microbes. Ecol. Appl. 20: 1556-1568, doi: 10.1890/08-1881.1

Mueller, P., K. Jensen, and J.P. Megonigal. 2016. Plants mediate soil organic matter decomposition in response to sea level rise. Glob. Change Biol. 22: 404-414, doi: 10.1111/gcb.13082

Müller, V. 2001. Bacterial fermentation. Encyclopedia of Life Sciences, doi: 10.1038/npg.els.0001415

Nemergut, D. R., and others. 2013. Patterns and processes of microbial community assembly. Microbiol. Mol. Biol. Rev. 77: 342–356, doi:10.1128/MMBR.00051-12

Nielsen, L. P. 1992. Denitrification in sediment determined from nitrogen isotope pairing. FEMS Microbiol. Lett. 86, 357-362, doi: 10.1016/0378-1097(92)90800-4

Oksanen, J., and others. 2017. vegan: Community Ecology Package. R package version 2.3–0.

Osburn, M.R., A.L. Sessions, C. Pepe-Ranney, and J.R. Spear. 2011. Hydrogen-isotopic variability in fatty acids from Yellowstone National Park hot spring microbial communities. Geochim. Cosmochim. Acta 75: 4830–4845, doi: 10.1016/j.gca.2011.05.038

Overbeek, R., and others. 2005. The subsystems approach to genome annotation and its use in the project to annotate 1000 genomes. Nucleic Acids Res. 33: 5691–5702, doi:10.1093/nar/gki866

Pallud, C. and P. Van Cappellen. 2006. Kinetics of microbial sulfate reduction in estuarine sediments. Geochim. Cosmochim. Acta 70: 1148–1162, doi: 10.1016/j.gca.2005.11.002

Pallud, C., C. Meile, A.M. Laverman , J. Abell J, and P. Van Cappellen. 2007. The use of flow-through sediment reactors in biogeochemical kinetics: methodology and examples of applications. Mar. Chem. 106: 256–271, doi: 10.1016/j.marchem.2006.12.011

Paluski, J.D. 1986. The release of reducing sugars and dissolved organic carbon from Spartina alterniflora Loisel in a Georgia salt marsh. Estuarine, Coastal Shelf Sci. 22: 385-394, doi:10.1016/0272-7714(86)90063-6

Parks, D.H. and R.G. Beiko. 2010. Identifying biologically relevant differences between metagenomic communities. Bioinformatics 26: 715-721, doi: 10.1093/bioinformatics/btq041

Perry, G. J., J. K. Volkman, R. B. Johns, and H. J. Bavor. 1979. Fatty acids of bacterial origin in contemporary marine sediments. Geochim. Cosmochim. Acta 43: 1715–1725, doi:10.1016/0016-7037(79)90020-6

Petushkova, E., S. Iuzhakov, and A. Tsygankov. 2019. Differences in possible TCA cycle replenishing pathways in purple non-sulfur bacteria possessing glyoxylate pathway. Photosyn. Res. 139: 523-537, doi: 10.1007/s11120-018-0581-1

Peyraud, R., P. Kiefer, P. Christen, S. Massou, J.-C. Portais, and J. A. Vorholt. 2009. Demonstration of the ethylmalonyl-CoA pathway by using 13C metabolomics. Proc. Nat. Acad. Sci. U.S.A. 106: 4846–4851, doi:10.1073/pnas.0810932106

Postgate, J. R. 1982. The fundamentals of nitrogen fixation. CUP Archive.

Powell, J. R., A. Welsh, and S. Hallin. 2015. Microbial functional diversity enhances predictive models linking environmental parameters to ecosystem properties. Ecology 96: 1985–1993, doi:10.1890/14-1127.1

Prosser, J. I., and others. 2007. The role of ecological theory in microbial ecology. Nat. Rev. Microbiol. 5: 384–392, doi:10.1038/nrmicro1643

Prosser, J. I. 2015. Dispersing misconceptions and identifying opportunities for the use of 'omics' in soil microbial ecology. Nat. Rev. Microbiol. 13: 439-446, doi: 10.1038/nrmicro3468

Quince, C., A.W. Walker, J.T. Simpson, N.J. Loman, and N. Segata. 2017. Shotgun metagenomics, from sampling to analysis. Nat. Biotechnol. 35: 833-844, doi: 10.1038/nbt.3935

R Core Team. 2013. R: A language and environmental for statistical computing. R Foundation for Statistical Computing, Vienna, Austria

Raghoebarsing, A. A., A. Pol, K. T. van de Pas-Schoonen, and others. 2006. A microbial consortium couples anaerobic methane oxidation to denitrification. Nature 440: 918–921, doi:10.1038/nature04617

Reed, D.C., C.K. Algar, J.A. Huber, and G.J. Dick. 2014. Gene-centric approach to integrating environmental genomics and biogeochemical models. Proc. Natl. Acad. Sci. U.S.A. 111: 1879–1884, doi:10.1073/pnas.1313713111

Roy, R. and R. Conrad. 1999. Effect of methanogenic precursors (acetate, hydrogen, propionate) on the suppression of methane production by nitrate in anoxic rice field soil. FEMS Microbiol. Ecol. 28: 49-61, doi: 10.1111/j.1574-6941.1999.tb00560.x

Ryther, J. H., and W.M. Dunstan. 1971. Nitrogen, phosphorus , and eutrophication in the coastal marine environment. Science 80: 1008–1013.

Scneider, K., R. Peyraud, P. Kiefer, P. Christen, N. Delmotte, S. Massou, J. C. Portais, and J.A. Vorholt. 2012. The ethylmalonyl-CoA pathway is used in place of the glyoxylate cycle by Methylobacterium extorquens AM1 during growth on acetate. J. Bio. Chem. 287: 757-766, doi: 10.1074/jbc.M111.305219

Setzke, E., R. Hedderich, S. Heiden, and R.K. Thauer. 1994. H2: heterodisulfide oxidoreductase complex from Methanobacterium thermoautotrophicum: composition and properties. Eur. J. Biochem., 220: 139-148, doi: 10.1111/j.1432-1033.1994.tb18608.x

Spivak, A.C. and J. Ossolinski. 2016. Limited effects of nutrient enrichment on bacterial carbon sources in salt marsh tidal creek sediments. Mar. Ecol. Prog. Ser. 554: 107-130, doi: 10.3354/meps11587

Solorzano, L. 1969. Determination of ammonia in natural waters by the phenolhypochlorite method. Limnol. Oceanogr. 14: 799-801, doi: 10.4319/lo.1969.14.5.0799

Strittmatter, A. W, and others. 2009. Genome sequence of Desulfobacterium autotrophicum HRM2, a marine sulfate reducer oxidizing organic carbon completely to carbon dioxide. Environ. Microbiol. 11: 1038–1055, doi:10.1111/j.1462-2920.2008.01825.x

Teal, J. and J. Kanwisher. 1961. Gas exchange in a Georgia salt marsh. Limnol Oceanogr 6: 388–399, doi: 10.4319/lo.1961.6.4.0388

Thamdrup, B., H. Fossing, and B.B. Jorgensen. 1994. Manganese, iron and sulfur cycling in a coastal marine sediment, Aarhus Bay, Denmark. Geochim. Cosmochim. Acta 58: 5115–5129, doi: 10.1016/0016-7037(94)90298-4

Thauer, R. K. 2011. Anaerobic oxidation of methane with sulfate: on the reversibility of the reactions that are catalyzed by enzymes also involved in methanogenesis from CO2. Curr. Opin. Microbiol. 14: 292–299, doi:10.1016/j.mib.2011.03.003

Thomas, F., A.E. Giblin, Z.G. Cardon, and S.M. Sievert. 2014. Rhizosphere heterogeneity shapes abundance and activity of sulfur-oxidizing bacteria in vegetated salt marsh sediments. Front. Microbiol. 5: 309, doi:10.3389/fmicb.2014.00309

van Dijk, E. L., H. Auger, Y. Jaszczyszyn, and C. Thermes. (2014). Ten years of next-generation sequencing technology. Trends Genet. 30: 418–426, https://doi.org/10.1016/j.tig.2014.07.001

Volkman, J. K., S.W. Jeffrey, P.D. Nichols, G.I. Rogers, and C.D. Garland. 1989. Fatty acid and lipid composition of 10 species of microalgae used in mariculture. J. Exp. Mar. Biol. Ecol. 128: 219-240, doi: 10.1016/0022-0981(89)90029-4

Vu, V.Q. 2011. ggbiplot: A ggplot2 based biplot R package version 0.55.

Wallenstein, M. D. and E. K. Hall. 2012. A trait-based framework for predicting when and where microbial adaptation to climate change will affect ecosystem functioning. Biogeochemistry 109: 35–47, doi:10.1007/s10533-011-9641-8

Westrich, J.T., and R.A. Berner. 1984. The role of sedimentary organic matter in bacterial sulfate reduction: The G model tested. Limnol. Oceanogr. 29: 236–249, doi:10.4319/lo.1984.29.2.0236

Wickham, H. 2016. Ggplot2: elegant graphics for data analysis. Springer Nature

Wikström, M. and G. Hummer. 2012. Stoichiometry of proton translocation by respiratory complex I and its mechanistic implications. Proc. Nat. Acad. Sci. 109: 4431-4436, doi: 10.1073/pnas.1120949109

Wilson, C.A., Z.J. Hughes, D.M. FitzGerald, C.S. Hopkinson, V. Valentine, and A.S. Kolker. 2014. Saltmarsh pool and tidal creek morphodynamics: dynamic equilibrium of northern latitude saltmarshes? Geomorphology 213: 99–115, doi: 10.1016/j.geomorph.2014.01.002

Wilson, W. A., P. J. Roach, M. Montero, E. Baroja-Fernández, F. J. Muñoz, G. Eydallin, A. M. Viale, and J. Pozueta-Romero. 2010. Regulation of glycogen metabolism in yeast and bacteria. FEMS Microbiol. Rev. 34: 952–985, doi:10.1111/j.1574-6976.2010.00220.x

Woese, C. R. and G.E. Fox. 1977. Phylogenetic structure of the prokaryotic domain: the primary kingdoms. Proc. Natl. Acad. Sci. U.S.A. 74: 5088-5090, doi: 10.1073/pnas.74.11.5088

Yan, Z., M. Wang, and J.G. Ferry. 2017. A Ferredoxin- and F 420 H 2 -Dependent, Electron-Bifurcating, Heterodisulfide Reductase with Homologs in the Domains Bacteria and Archaea. mBio 8: e02285-16, doi:10.1128/mBio.02285-16

Yin, G., L. Hou, M. Liu, Z. Liu, and W. S. Gardner. 2014. A novel membrane inlet mass spectrometer method to measure15NH4+ for isotope-enrichment experiments in aquatic ecosystems. Environ. Sci. Technol. 48: 9555–9562, doi:10.1021/es501261s

Zedler, J.B. and S. Kercher. 2005. Wetland resources: status, trends, ecosystem services, and restorability. Annu. Rev. Environ. Resour. 30: 39–74, doi: 10.1146/annurev.energy.30.050504.144248

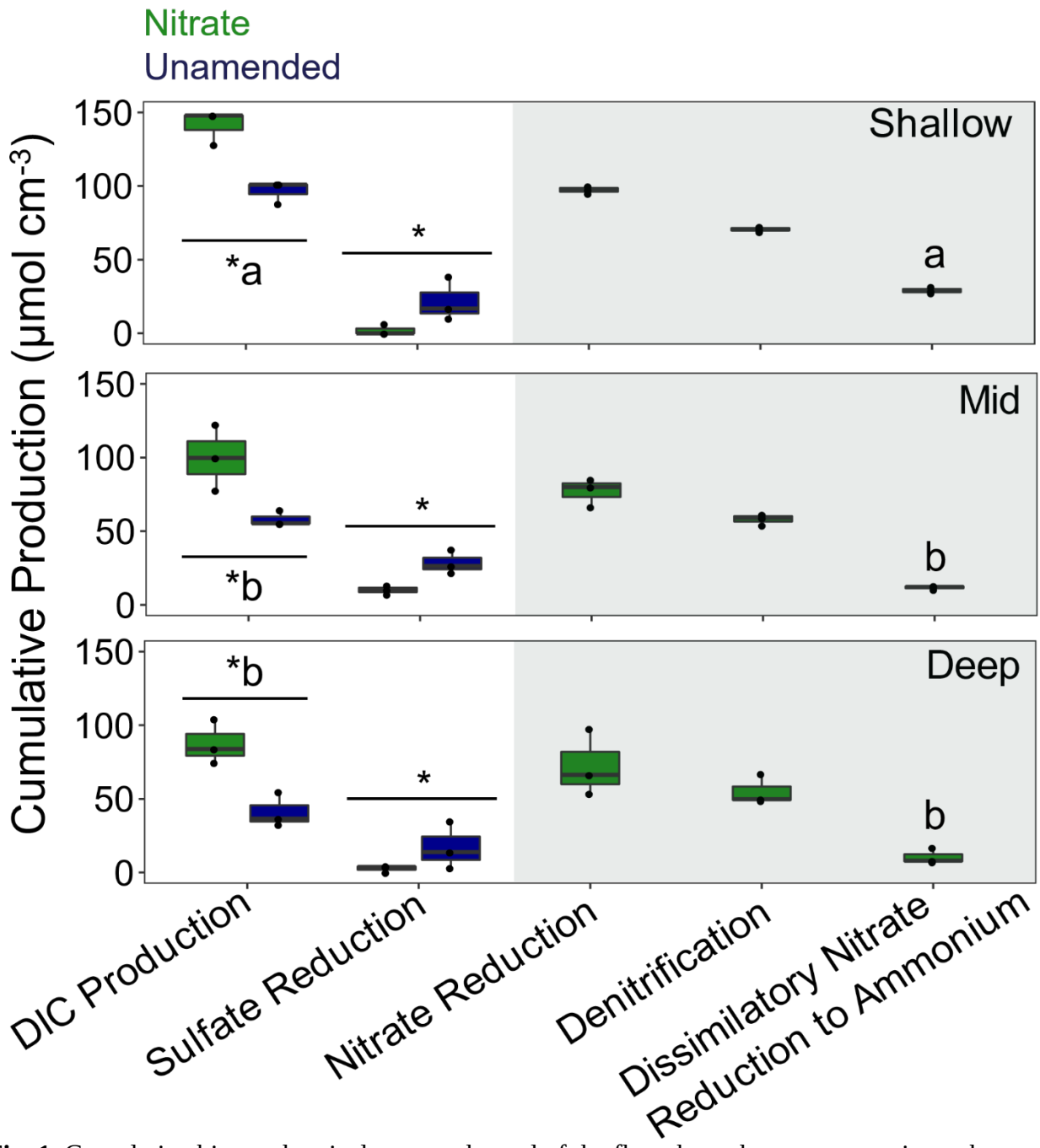

Fig. 1. Cumulative biogeochemical rates at the end of the flow through reactor experiment by treatment (color) and depth (panel). Each point represents a reactor replicate, with three replicates per treatment-depth combination (these points overlap in some cases due to small

variation). Processes in the gray box were either only detectable (NO_3^- reduction) or measured (denitrification and DNRA) in the NO_3^- treatment. Asterisks (*) indicate differences between treatments while letters indicate differences among depths within a rate measurement.

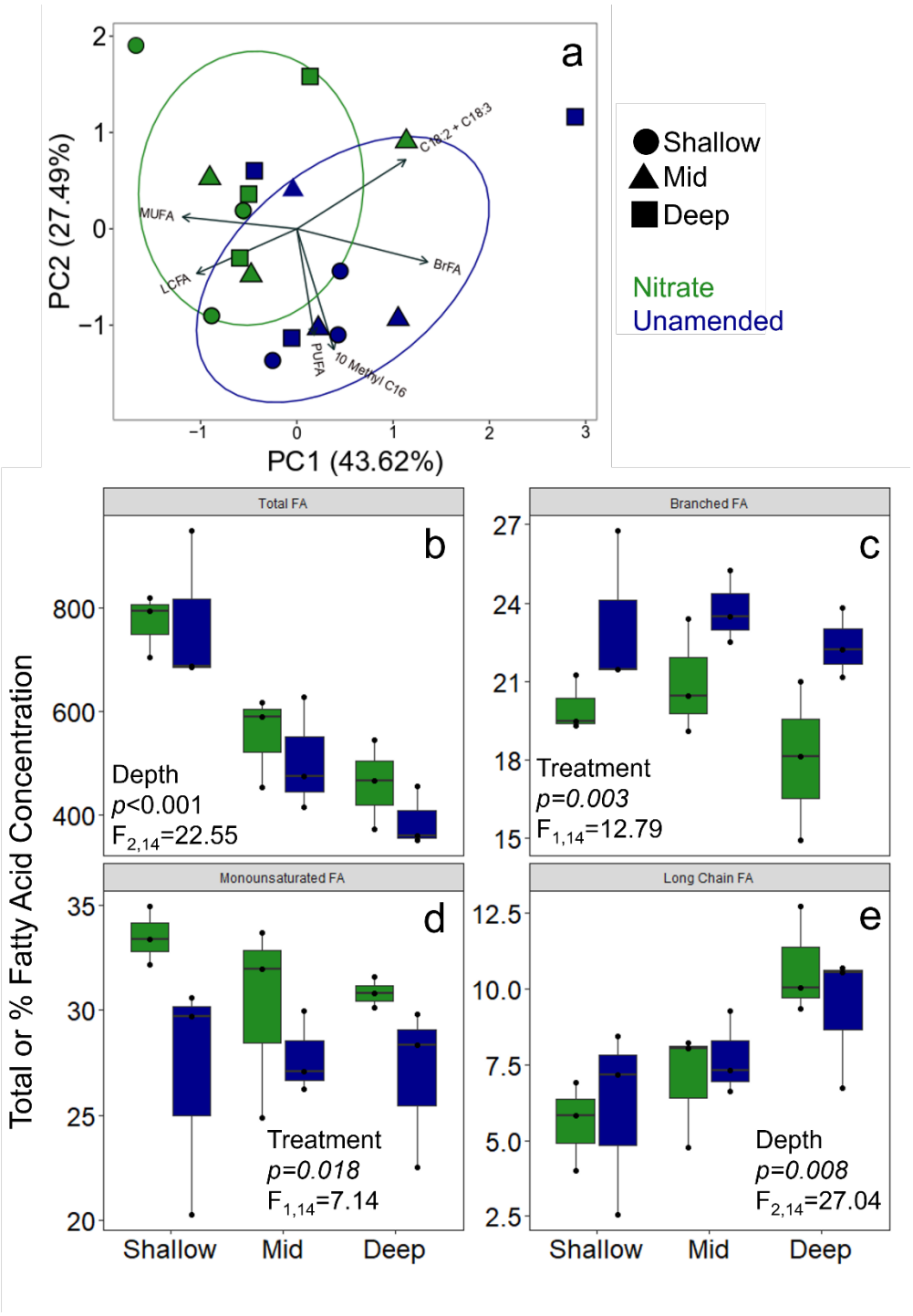

Fig. 2. (a) Results from principal component analysis (PCA) colored by treatment and categorized using normal probability ellipsoids. Box plots colored by treatment of (b) PLFAs (µg per g TOC), (c) bacteria (iso- and anteiso- branched $C_{13:0}$+$C_{15:0}$+$C_{17:0}$+$C_{19:0}$; BrFA), (d) microbes (monounsaturated FAs $C_{16:1}$+$C_{17:1}$+$C_{18:1}$+$C_{19:1}$; MUFA), and (e) vascular plants (long chain FAs $C_{24:0}$+$C_{26:0}$+$C_{28:0}$+$C_{30:0}$; LCFA and $C_{18:2}$ + $C_{18:3}$).

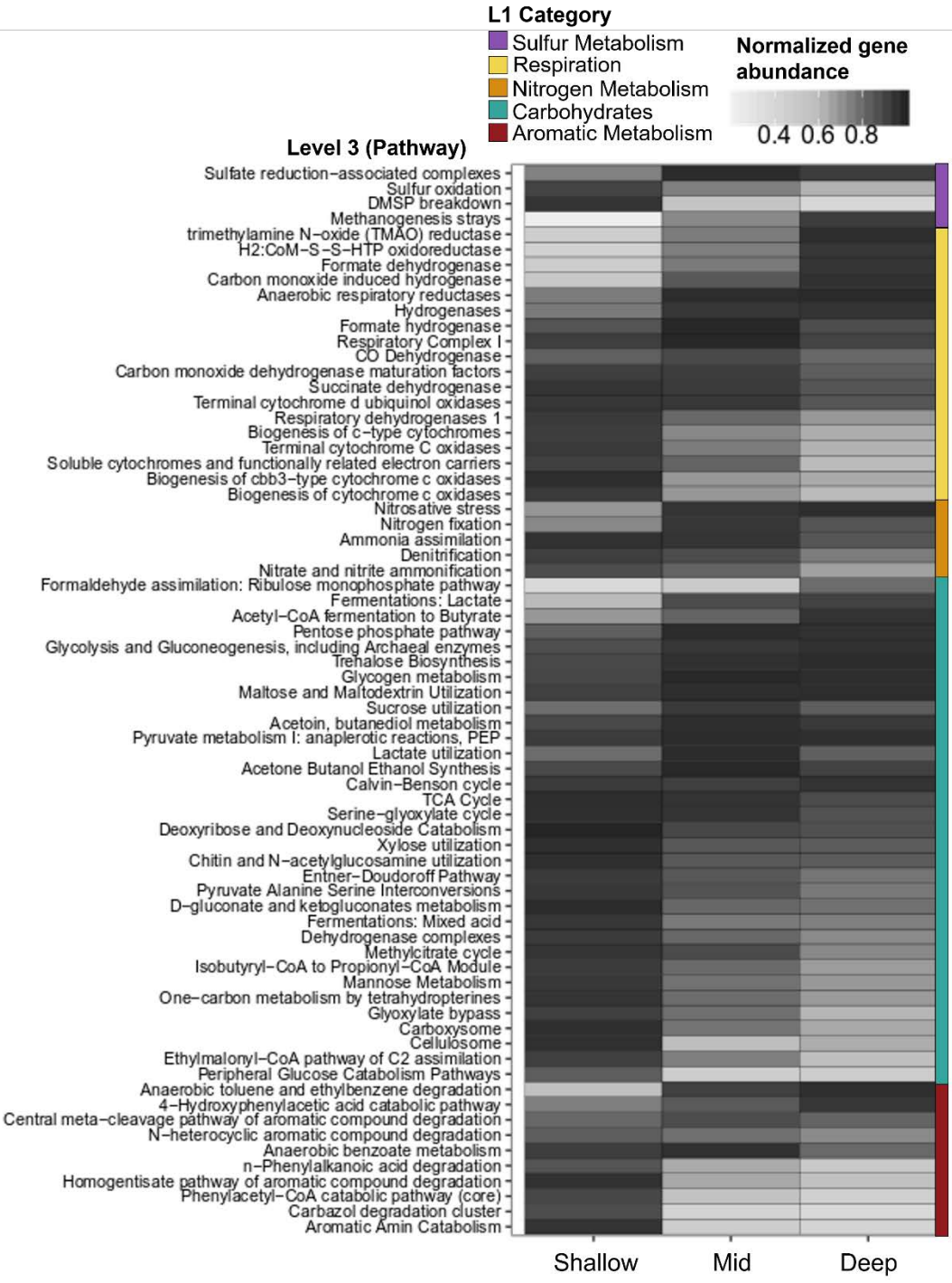

Fig. 3. Heatmap showing average normalized abundance of L3 functions (SEED subsystems) in pre-treatment sediments that are significantly different among depths according to a one-way ANOVA corrected by Benjamini-Hochberg FDR in STAMP. Colored bars represent the L1 categories associated with each of the L3 functions.

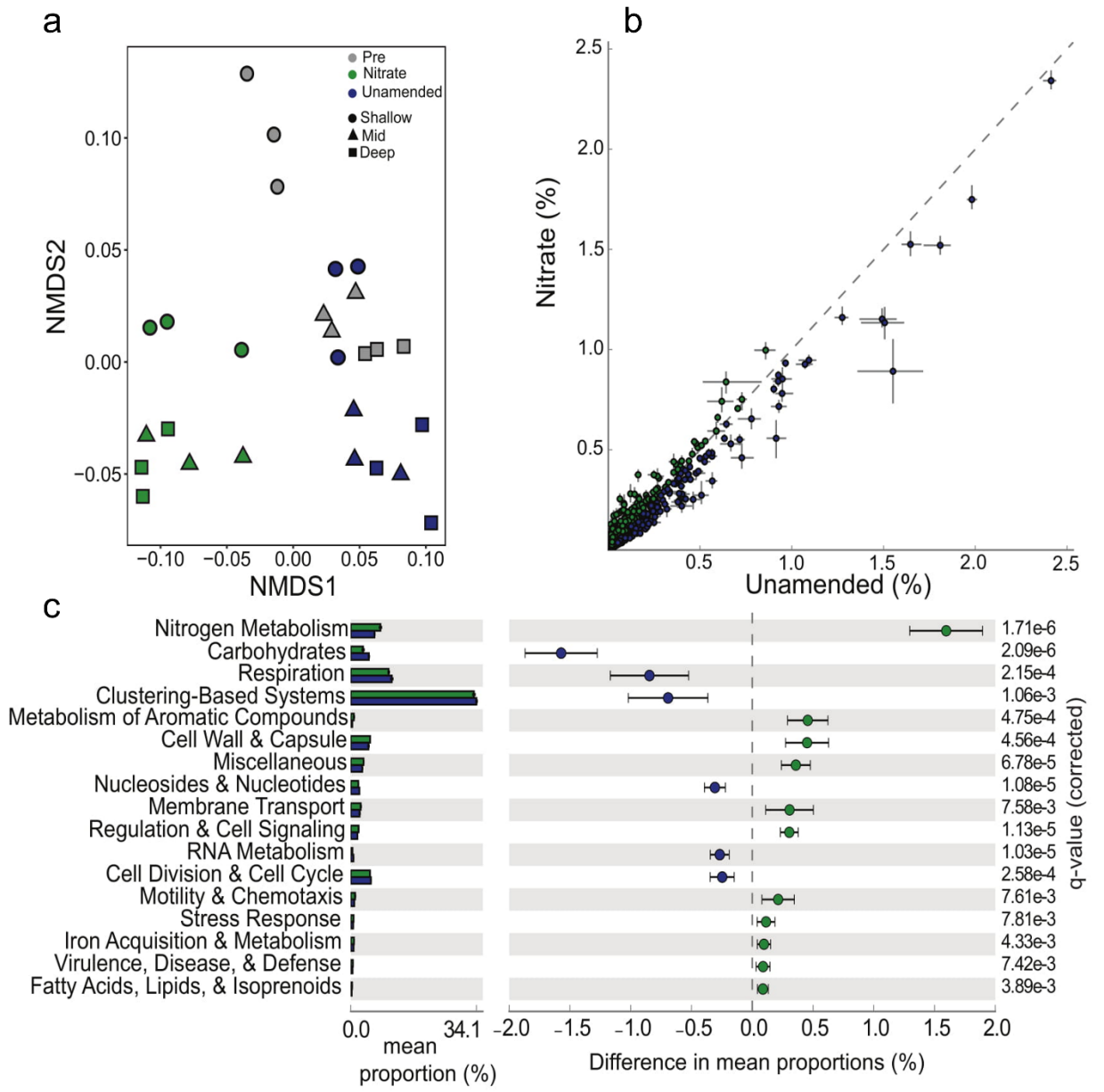

Fig. 4. (a) A non-metric multidimensional scaling plot of SEED subsystems level 1 functional annotations shows significant differences by treatment (color) and depth (shape) (b) A scatter plot of SEED subsystems level 4 functional annotation (561 features), where each point represents the relative proportion of unique gene abundances ± 25th and 75th percentile, shows clear separation between NO_3^- and unamended treatments. (c) An extended bar plot of 95% confidence intervals and mean proportion (%) shows significant differences between SEED

subsystem level 1 annotations for NO_3^- and unamended treatments as indicated by a q-value from the Benjamini-Hochberg FDR correction in STAMP.

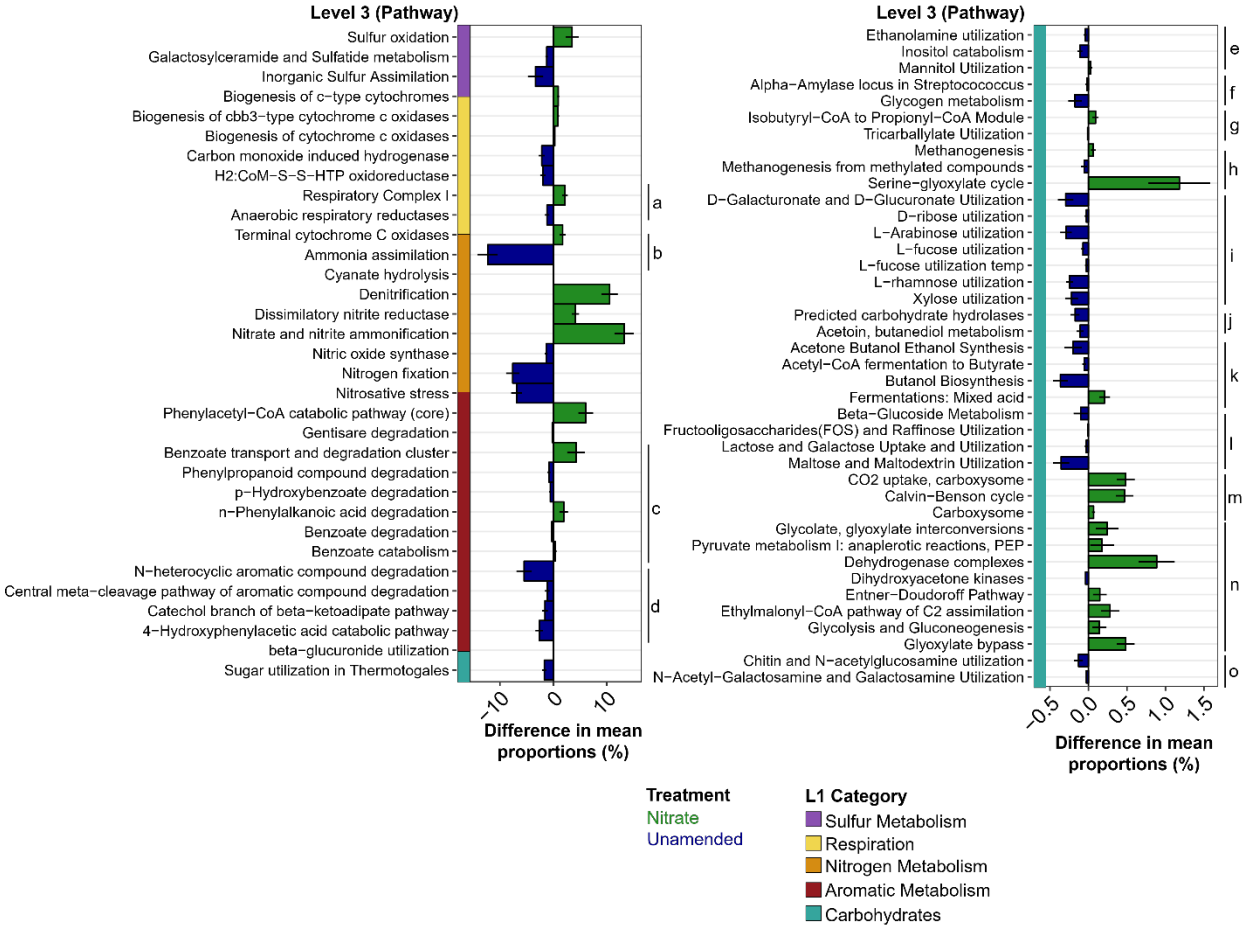

Fig. 5. Bar plot showing the average (±SD) difference in mean proportions (%) of L3 functions (SEED subsystems) that are significantly different by treatment according to a two-sample Welch's t-test corrected by Benjamini-Hochberg. Note the difference in scale between left and right plots. Colored bars along the left of each bar plot represents the L1 category and letters indicate corresponding L2 subcategories (a = electron donating reactions, b = electron accepting reactions, c = peripheral pathways for catabolism of aromatic compounds, d = metabolism of central aromatic intermediates, e = sugar alcohols, f = polysaccharides, g = organic acids, h = one-carbon metabolism, i = monosaccharides, j = glycoside hydrolases, k = fermentation, l = di- and oligosaccharides, m = CO_2 fixation, n = central carbohydrate metabolism, and o = aminosugars.

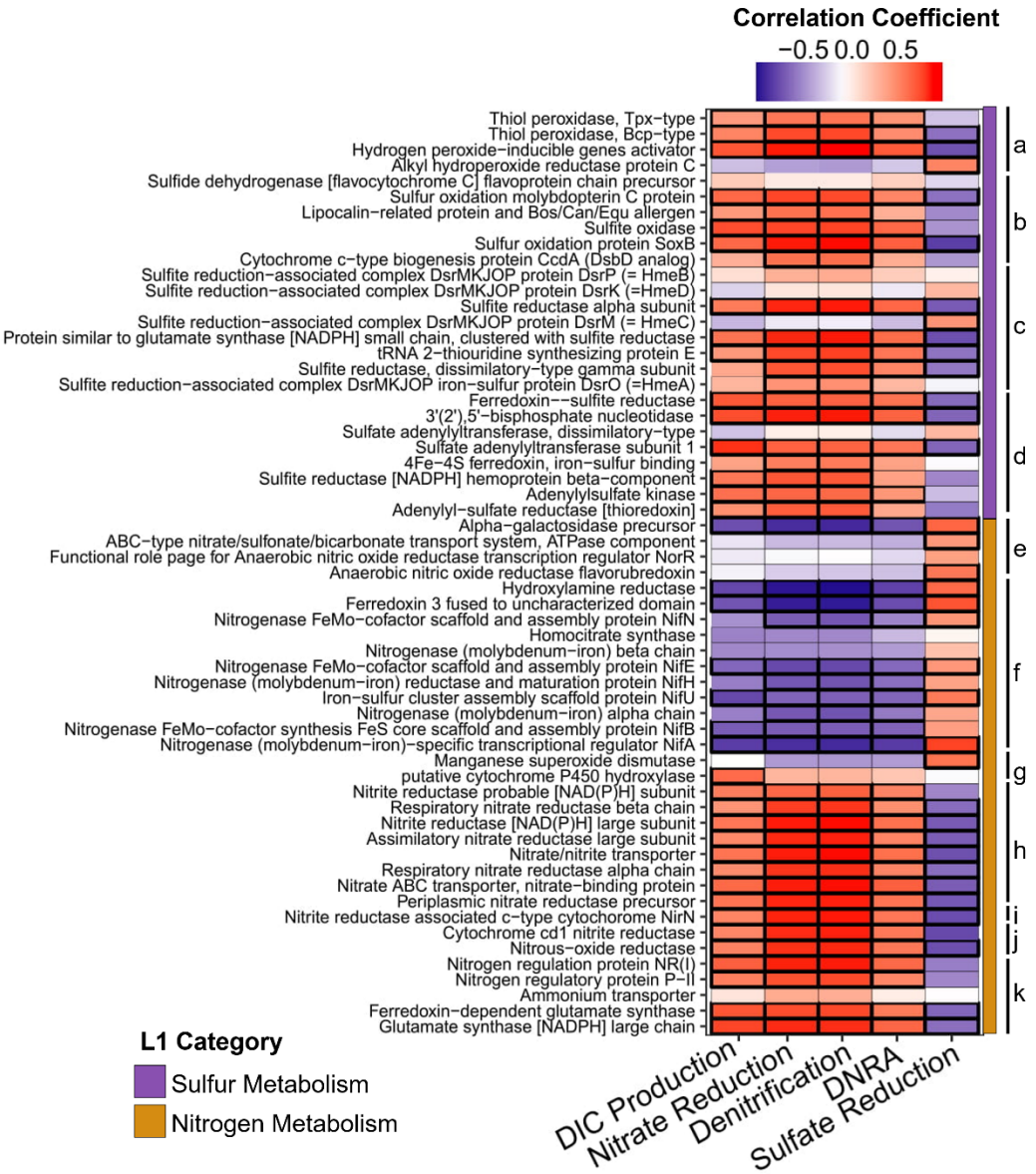

Fig. 6. Heatmap of Pearson's correlation coefficients between L4 functions within nitrogen and sulfur metabolisms (colored bars) and cumulative rates (μmol cm^{-3}) measured at the end of the flow through reactor experiment. Red and blue color codes represent positive and negative correlations, respectively, with black boxes indicating significant (p<0.05) correlations. Letters indicate L3 functional subsystems within which each L4 assignment resides (a = Thioredoxin-disulfide reductase, b = sulfur oxidation, c = sulfate reduction associated complexes, d = inorganic sulfur assimilation, e = nitrosative stress, f = nitrogen fixation, g = nitric oxide

synthase, h = NO_3^-/ NO_2^- ammonification, i = dissimilatory NO_3^- reductase, j = denitrification, k = ammonia assimilation). Detailed statistical results can be found in Table S5-9.

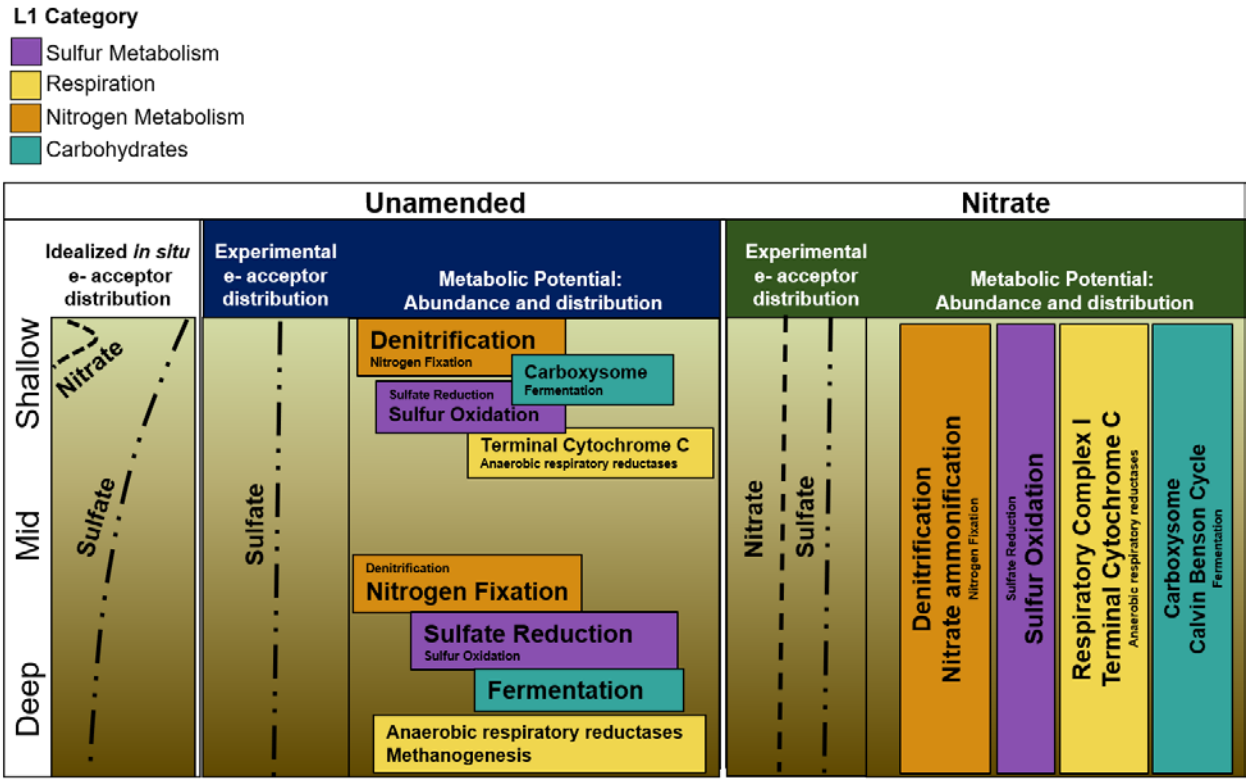

Fig. 7. Conceptual diagram describing patterns in Level 3 subsystems observed by depth in the unamended (left) and NO_3^- treatment (right). Text size represents the qualitative representation of subsystem abundance, with larger text indicating higher abundance, and colored boxes representing Level 1 categories within which these groups are categorized. The profile on the left describes the idealized and experimental electron acceptor distributions along depth gradients used in this study (shallow 0-5 cm; mid 10-15 cm; deep 20-25 cm), with increasing accumulation of less biologically OM in deeper sediments.